JCTC Journal of Chemical Theory and Computation

Article

pubs.acs.org/JCTC

A General Route to Include Pauli Repulsion and Quantum Dispersion Effects in QM/MM Approaches

Tommaso Giovannini, Piero Lafiosca, and Chiara Cappelli*

Scuola Normale Superiore, Piazza dei Cavalieri 7, 56126 Pisa, Italy

Supporting Information

ABSTRACT: A methodology to account for nonelectrostatic interactions in Quantum Mechanical (QM)/Molecular Mechanics (MM) approaches is developed. Formulations for Pauli repulsion and dispersion energy, explicitly depending on the QM density, are derived. Such expressions are based on the definition of an auxiliary density on the MM portion and the Tkatchenko−Scheffler (TS) approach, respectively. The developed method is general enough to be applied to any QM/MM method and partition, provided an accurate tuning of a small number of parameters is obtained. The coupling of the method with both nonpolarizable and fully polarizable QM/fluctuating charge (FQ) approaches is reported and applied. A suitable parametrization for the aqueous solution, so that its most representative features are well reproduced, is outlined. Then, the obtained parametrization and method are applied to calculate the nonelectrostatic (repulsion and dispersion) interaction energy of nicotine in aqueous solution.

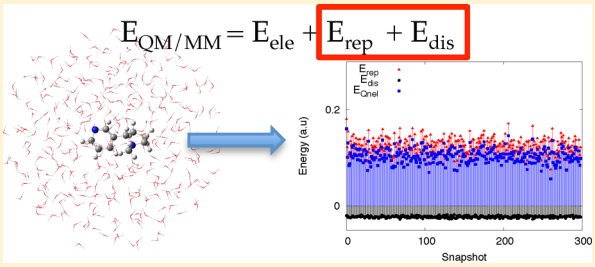

1. INTRODUCTION

Multiscale computational approaches rooted in the so-called hybrid quantum mechanics (QM)−molecular mechanics (MM) methods (QM/MM)[1−9] have nowadays been amply and successfully applied to a variety of chemical systems and their physicochemical properties.[10−20]

The idea behind those approaches is to treat accurately, by QM methods, a small but critical part of the overall system, while resorting to much cheaper and less accurate MM methods for the remaining portion of the whole system. Such a partition is sometimes naturally applicable (such as in solvation phenomena and noncovalent interactions); however, in some cases (i.e., covalently bound systems) the QM and MM portions are more difficult to define. In any case, a specific choice of the QM/MM partition introduces some assumptions on the system, which in the worst cases can negatively affect the quality of the final computed results. The quality of the results which can be obtained with QM/MM models do not only depend on the definition of the two moieties but also (and crucially) on the approach exploited to model the interaction between the two portions.[8,9]

Different choices are possible in this context; however, the model for the QM/MM coupling must be capable of treating both bonded and nonbonded interactions (electrostatic and nonelectrostatic). The way of treating the electrostatic interaction is generally a key element of any QM/MM approach, largely affecting the quality of the computed results.[9,21−24] Two groups of methods exist, the so-called mechanical embedding schemes and the electrostatic embedding methods.[25] The latter may not include mutual polarization effects between the QM and MM portions: in the first case, a set of atomic-centered partial point charges is used for calculating the electrostatic interaction at the MM level, which also enters in definition of the effective QM Hamiltonian. Polarization effects can be included by using either fluctuating charges (FQ),[26,27] distributed multipoles,[28−30] induced dipoles,[23,31,32] or Drude oscillators.[33]

Limiting QM/MM interactions to electrostatic-only terms may yield an unphysical description of the systems. Nonelectrostatic interactions,[34] also called London interactions, play a crucial role in many chemical processes. For instance, most of the DNA and RNA functionalities, as well as the adsorption of a molecule on a surface are regulated by repulsion/dispersion interactions. Moreover, these interactions can also play an important role in solvation phenomena.

Although they have paramount importance, in most QM/MM approaches nonelectrostatic interactions between the QM and MM moieties are only retained at the MM level and treated by means of Lennard-Jones or similar parametrized analytical functions.[35]

This approach, if computationally inexpensive, introduces a rough approximation in the computational modeling. In fact, nonelectrostatic interactions are primarily due to the Pauli repulsion principle, which cannot be postulated in a classical framework, and to long-range electron correlation effects, which are again not defined in the classical realm. In purely QM approaches, such interactions are modeled by resorting to correlated expensive QM methods, such as coupled cluster with single, double, and perturbative triple excitations—CCSD(T) coupled to large atomic basis sets in order to reduce the basis set superposition error (BSSE).[36,37]

Received: July 19, 2017
Published: September 12, 2017

DOI: 10.1021/acs.jctc.7b00776
J. Chem. Theory Comput. 2017, 13, 4854−4870

The formulation of QM/MM approaches able to account for QM effects affecting dispersion/repulsion interactions between the QM and MM portions has received so far only little attention in the literature. To the best of our knowledge, the only approach which has been proposed is the so-called effective fragment potential (EFP) method.[20,28,29,38−40] In this approach, empirical force fields are not exploited, but the force field (FF) for the "MM" portion is obtained from electronic structure calculations of the single fragments. In this way, the FF is defined in terms of point charges, multipoles, static and dynamic polarizabilities, localized molecular orbitals, and related QM quantities.

Due to the nature of the EFP method, the inclusion of dispersion and Pauli repulsion terms can be formulated in terms of QM quantities calculated for the fragments. Therefore, such an approach cannot be straightforwardly extended to generic QM/MM methods based on empirical potentials.

The account for QM-based nonelectrostatic interactions (explicitly depending on the QM density) in QM/MM calculations will not only permit a more reliable description of the interaction between the QM and the MM moieties but also include them in the QM Hamiltonian and propagate such terms also to molecular properties and spectra. The common approaches, based on Lennard-Jones and similar potentials, which do not bear any explicit dependence on QM quantities, do not give any contribution to the QM Hamiltonian; therefore they only result in a correction to the QM/MM energy. As it will be detailed in the following sections, the development of a model with the aforementioned features is the goal of this paper.

Notice that we do not aim to propose a way of decomposing the intermolecular energy terms. Such kinds of calculations can be performed by exploiting other approaches, for instance, the general effective fragment potential (EFP2)[20] or the symmetry adapted perturbation theory (SAPT)[41,42] approach.

The manuscript is organized as follows: first, a general formulation of Pauli repulsion and dispersion energy in a QM/MM framework is presented. The formulation that is reported is based on the definition of an auxiliary density on the MM portion and the Tkatchenko−Scheffler (TS) approach[43−46] for the repulsion and dispersion terms, respectively. Next, the inclusion of such terms in the QM/MM Hamiltonian is derived, with specific emphasis in the coupling with the polarizable QM/MM approach which is developed in our group.[13,24,27,47−49] The derived repulsion/dispersion terms depend on some parameters. A parametrization to treat aqueous solution is then proposed, which allows the application of the methodology to treat nonelectrostatic interaction energies of solvated systems. To this end, aqueous solutions of (L)-methyl lactate (MLAT) and (R)-methyloxirane (MOXY) are considered, as well as the more complicated case of nicotine in aqueous solution, where the focus is on the influence of nonelectrostatic interactions on conformational populations and on the electric dipole. Summary, conclusions, and future perspectives end the presentation.

2. THEORY

The total energy of a system composed by two interacting moieties A and B can be expressed as[50,51]

$$E_{AB} = E_{AB}^{ele} + E_{AB}^{pol} + E_{AB}^{pen} + E_{AB}^{ex} + E_{AB}^{dis} \quad (1)$$

where E_{AB}^{ele} arises from electrostatic interactions and E_{AB}^{pol} is the polarization contribution. E_{AB}^{pen} is the so-called penetration term, E_{AB}^{ex} is the exchange contribution, and E_{AB}^{dis} arises from dispersion interactions. In the context of QM/MM approaches, A can represent the QM portion of the system, and B the MM one. E_{AB}^{ele} and E_{AB}^{pol} are the energy terms considered within electrostatic embedding schemes and in particular in polarizable QM/MM approache.s[1,8,23,27,31−33]

2.1. Pauli Repulsion Energy. The Pauli repulsion energy, E_{AB}^{rep}, also known as exchange-repulsion energy, is formally the sum between the penetration (E_{AB}^{pen}) and the exchange (E_{AB}^{ex}) contributions in eq 1 above. The penetration term is considered to be twice the exchange term in the van der Waals region, thus giving rise to the following expression:[51,52]

$$E_{AB}^{rep} = \frac{1}{2}\int \frac{d\mathbf{r}_1\, d\mathbf{r}_2}{r_{12}} \rho_A(\mathbf{r}_1, \mathbf{r}_2)\, \rho_B(\mathbf{r}_2, \mathbf{r}_1) \quad (2)$$

where ρ_x is the density matrix of the A or B moieties, placed at distance r_{12}.

The extension of eq 2 to QM/MM partitions is obstructed by the difficulty to define the density matrix ρ_B of the classical region B (no electrons are present in this region).

In the following derivation, we will work out an approximate expression for Pauli repulsion in the framework of the so-called focused models,[53] namely models in which the main component, that essentially bearing the property, is described at a higher level than the remainder, which plays a complementary but not negligible role. Within such an approach, terms related to two fragments of the MM portion are not considered.

The starting point for the derivation of the equations is the formulation of quantum repulsion effects for the polarizable continuum model.[52,54−56] In particular, each fictitious valence electron pair of the MM molecules is localized in bond and lone pair (if they are present) regions and represented by an s-Gaussian-type function. Due to the different physical nature of the two (bond or lone pair) regions, the two are discerned by using two different sets of parameters, so that the expression for ρ_B becomes[52]

$$\rho_{MM}(\mathbf{r}_1, \mathbf{r}_2) = \sum_{\mathbf{R}} \xi_{\mathbf{R}}^2\, e^{-\beta_{\mathbf{R}}(\mathbf{r}_1-\mathbf{R})^2} \cdot e^{-\beta_{\mathbf{R}}(\mathbf{r}_2-\mathbf{R})^2} \quad (3)$$

where $\mathbf{R}$ collects the centers of the Gaussian functions used to represent the fictitious MM electrons. The β and ξ parameters are generally different for lone pairs or bond pairs: their values are adjusted to the specific kind of environment (MM portion) to be modeled (vide infra). By substituting eq 3 in eq 2, the QM/MM repulsion energy reads

$$E_{QM/MM}^{rep} = \frac{1}{2}\sum_{\mathbf{R}} \int \frac{d\mathbf{r}_1\, d\mathbf{r}_2}{r_{12}} \rho_{QM}(\mathbf{r}_1, \mathbf{r}_2)\left[\xi_{\mathbf{R}}^2\, e^{-\beta_{\mathbf{R}}(\mathbf{r}_1-\mathbf{R})^2} \cdot e^{-\beta_{\mathbf{R}}(\mathbf{r}_2-\mathbf{R})^2}\right] \quad (4)$$

In this formalism, the QM/MM Pauli repulsion energy is calculated as a two-electron integral. Interestingly, this differs from the formulation of the same quantity in the PCM model,[52] where this term is a pure one-electron term.

Eq 4 holds for every kind of MM environment, independent from its nature; i.e., the formalism not only holds for solvents but can be extended to other substrates (proteins, surfaces) surrounding the QM core region. The specification for the different external environments is simply done by defining the number of different electron-pair types and the relative β and ξ parameters in eq 3. Also, due to its simplicity, this formalism is retained also in the case of polarizable QM/MM approaches, such as our polarizable QM/fluctuating charge (FQ) approach[49] (vide infra), by only refining the parameters if necessary. To end

DOI: 10.1021/acs.jctc.7b00776
J. Chem. Theory Comput. 2017, 13, 4854−4870

the discussion, it is worth noticing that in the present work ρ_{MM} will only be defined in terms of spherical Gaussian-type functions. Extension to p/d-type functions is possible and mainly implies the definition of additional parameters in eq 3. Such an extension (and the related parametrization work) will be the topic of future communications.

2.1.1. Practical Formulation of $E^{rep}_{QM/MM}$. As pointed out above, eq 4 requires the calculation of a two-electron integral. Such an integral is formally similar to the exchange integral (with opposite sign), where one of the densities in eq 2 has been replaced with an explicit function of $\mathbf{r}_1$ and $\mathbf{r}_2$. A similar approach is sometimes used within the framework of density functional theory (DFT), in the development of hybrid density functionals with a nonlocal contribution to the energy. Similar to the definition of the exchange term, in DFT an exchange-repulsion energy density can be defined:[57]

$$\varepsilon^{rep}(\mathbf{r}_1) = \frac{1}{2}\int d\mathbf{u}\frac{\rho_{QM}(\mathbf{r}_1, \mathbf{r}_1+\mathbf{u})\,\rho_{MM}(\mathbf{r}_1, \mathbf{r}_1+\mathbf{u})}{u} \tag{5}$$

where $\mathbf{u} = \mathbf{r}_2 - \mathbf{r}_1$ has been introduced (u is its module). In this formalism, ρ_{MM} acts as a "semilocal density" in the DFT framework.[57−61] By inserting ρ_{MM} in eq 5, we obtain

$$\varepsilon^{rep}(\mathbf{r}_1) = \frac{1}{2}\int d\mathbf{u}\frac{\rho_{QM}(\mathbf{r}_1, \mathbf{r}_1+\mathbf{u})}{u}\left(\sum_{\mathbf{R}} \xi_{\mathbf{R}}^2\, e^{-\beta_{\mathbf{R}}|\mathbf{r}_1-\mathbf{R}|^2}\, e^{-\beta_{\mathbf{R}}|\mathbf{r}_1+\mathbf{u}-\mathbf{R}|^2}\right) \tag{6}$$

By exploiting the standard approach of expanding a non-interacting reference system's Kohn−Sham orbitals in a finite basis set of real, nonorthogonal, Gaussian-type atomic orbitals $\{\chi_\mu\}$, the nonlocal one-particle density becomes

$$\rho_{QM}(\mathbf{r}_1, \mathbf{r}_1+\mathbf{u}) = \sum_{\mu\nu} P_{\mu\nu}\chi_\mu(\mathbf{r}_1)\,\chi_\nu(\mathbf{r}_1+\mathbf{u}) \tag{7}$$

where $P_{\mu\nu}$ is the μ,ν element of the density matrix $\mathbf{P}$. By substituting eq 7 into eq 6, and symmetrizing, to recover the notation of Rung 3.5 functionals, $\varepsilon^{rep}(\mathbf{r}_1)$ becomes

$$\varepsilon^{rep}(\mathbf{r}_1) = \frac{1}{2}\sum_{\mu\nu} P_{\mu\nu}\left[\frac{\chi_\mu(\mathbf{r}_1)\,A_\nu(\mathbf{r}_1) + A_\mu(\mathbf{r}_1)\,\chi_\nu(\mathbf{r}_1)}{2}\right] \tag{8}$$

where similarly to what is done in the context of the definition of the so-called "hybrid Rung 3.5 density functionals"[61−64] the A_μ function is introduced:

$$A_\mu(\mathbf{r}_1) = \int d\mathbf{u}\frac{\chi_\mu(\mathbf{r}_1+\mathbf{u})}{u}\left(\sum_{\mathbf{R}} \xi_{\mathbf{R}}^2 e^{-\beta_{\mathbf{R}}|\mathbf{r}_1-\mathbf{R}|^2} e^{-\beta_{\mathbf{R}}|\mathbf{r}_1+\mathbf{u}-\mathbf{R}|^2}\right) \tag{9}$$

Eq 9 has the form of an electrostatic potential integral, yielding the potential at point $\mathbf{r}_1$ due to the product of a basis function centered at $\mathbf{R}_\mu$ and the sum of the Gaussian functions representing ρ_{MM}, centered at $\mathbf{R}$. Such an integral can be calculated analytically, for instance, by specifying the Obara-Saika algorithm[65−67] to the evaluation of eq 9. The details on the formulation and implementation of this algorithm in the context of the present work are given as Supporting Information (SI; section S1). Notice, however, that a straightforward adaption of the current implementations of Rung 3.5 density functionals[61−64] to the evaluation of eq 9 is impossible. In addition, the definition of ρ_{MM} (eq 3) does not allow the use of the auxiliary basis sets exploited in Rung 3.5 functionals, because the Gaussian functions which we are using (eq 3) are centered in the MM grid. Since they are by definition nonsymmetric functions, the Müntz theorem[68] cannot be applied to our case.

By rewriting eq 9 as a function of $\mathbf{r}_2$:

$$A_\mu(\mathbf{r}_1) = \sum_{\mathbf{R}} \xi_{\mathbf{R}}^2\, e^{-\beta_{\mathbf{R}}|\mathbf{r}_1-\mathbf{R}|^2}\int d\mathbf{r}_2\frac{\chi_\mu(\mathbf{r}_2)\, e^{-\beta_{\mathbf{R}}|\mathbf{r}_2-\mathbf{R}|^2}}{|\mathbf{r}_2-\mathbf{r}_1|} \tag{10}$$

the exchange-repulsion energy, $E^{rep}_{QM/MM}$, can be calculated by numerical integration of the energy density in eq 8:

$$E^{rep}_{QM/MM} = \frac{1}{2}\sum_{\mu\nu} P_{\mu\nu}\int d\mathbf{r}_1\left[\frac{\chi_\mu(\mathbf{r}_1)\,A_\nu(\mathbf{r}_1) + A_\mu(\mathbf{r}_1)\,\chi_\nu(\mathbf{r}_1)}{2}\right] \tag{11}$$

and the matrix element of the Pauli-repulsion potential, to be added to the QM Fock matrix, reads

$$F^{rep}_{\mu\nu} = \frac{\partial E^{rep}}{\partial P_{\mu\nu}} = \frac{1}{2}\int d\mathbf{r}_1\left[\frac{\chi_\mu(\mathbf{r}_1)\,A_\nu(\mathbf{r}_1) + A_\mu(\mathbf{r}_1)\,\chi_\nu(\mathbf{r}_1)}{2}\right] \tag{12}$$

It is worth remarking that the resorting to the DFT formalisms allows to transform the two-electron integral in eq 4 into a one-electron integral, which can be evaluated by integration over grid points defined in the DFT formalism.

Also, eq 11 depends explicitly on both $P_{\mu\nu}$ and the atomic basis $\{\chi_\mu\}$. This introduces an explicit contribution to the QM Hamiltonian, which propagates to the calculation of molecular properties and spectra, through the definition of suitable analytical procedures. Such an extension will be the topic of further investigations.

2.2. Quantum Dispersion Energy. The exact quantum-mechanical definition of the dispersion interaction originally proposed by McWeeny results in a computationally expensive approach, depending on transition densities of the QM portion.[51,69] A popular remedy to this issue, widely used in the case of dispersion corrected density functionals,[43,44,70−81] consists of adding a pairwise interatomic C_6R^{-6} term to the DFT energy:

$$E^{dis} = -\frac{1}{2}\sum_{A,B} f_{damp}(R_{AB}, R^0_A, R^0_B)C_{6AB}R^{-6}_{AB} \tag{13}$$

where R_{AB} is the distance between atoms (portions) A and B, C_{6AB} is the corresponding C_6 coefficient, and R^0_A and R^0_B are the van der Waals (vdW) radii. The R^{-6}_{AB} singularity at small distances is eliminated by the short-range damping function $f_{damp}(R_{AB}, R^0_A, R^0_B)$.

Among the several corrections proposed in the literature, we found the approach by Tkatchenko and Scheffler (TS) the most suitable for our purposes, due to its mathematical formulation and its performances.[43] Starting from the Casimir−Polder equation and the Padé series, the C_{6AB} coefficients are defined by only using homonuclear parameters, i.e., C_{6AA}, C_{6BB}, α^0_A, and α^0_B (the latter being static polarizabilities of the A and B moieties):

$$C_{6AB} = \frac{2C_{6AA}C_{6BB}}{\frac{\alpha^0_B}{\alpha^0_A}C_{6AA} + \frac{\alpha^0_A}{\alpha^0_B}C_{6BB}} \tag{14}$$

Similarly to repulsion, also for dispersion terms only the interaction between QM (A) and MM (B) atoms will be

DOI: 10.1021/acs.jctc.7b00776
J. Chem. Theory Comput. 2017, 13, 4854−4870

considered. The TS model resorts to an atom in molecules[82] approach and adopts the Hirshfeld[83] partition of the density to define effective homonuclear coefficients C_{6AA}^{eff} of the A atom in the molecule:

$$C_{6AA}^{eff} = \left(\frac{V_A^{eff}}{V_A^{free}}\right)^2 C_{6AA}^{free} = \eta_A^2 C_{6AA}^{f} \tag{15}$$

where (V_A^{eff}) is the effective volume of the A atom in the molecule, (V_a^{free}) is the free volume of the same atom, and C_{6AA}^{free} are the free homonuclear coefficients C_{6AA}^{free}. η_A can be written in terms of the electron density of the system by employing the Hirshfeld partitioning of the density:[83]

$$\eta_A = \frac{\int d\mathbf{r}\, r^3\, w_A(\mathbf{r})\, \rho(\mathbf{r})}{\int d\mathbf{r}\, r^3\, \rho_A^{free}(\mathbf{r})} \tag{16}$$

$$w_A(\mathbf{r}) = \frac{\rho_A^{free}(\mathbf{r})}{\sum_J \rho_J^{free}(\mathbf{r})} \tag{17}$$

where $w_A(\mathbf{r})$ is the Hirshfeld atomic partitioning weight for the atom A, r is the distance from the nucleus, $\rho(\mathbf{r})$ is the total electron density, $\rho_A^{free}(\mathbf{r})$ is the electron density of the free atom A, and the summation runs over all atoms J in the system.

By following this approach, the QM/MM dispersion energy, $E_{QM/MM}^{dis}$, becomes

$$E_{QM/MM}^{dis} = -\frac{1}{2}\sum_{A\in QM}\sum_{B\in MM} f_{damp}(R_{AB}, R_A^0, R_B^0)\, \frac{\eta_A^2 C_{AA}^{free} C_{6BB}^{eff}}{\frac{\alpha_B^0}{\alpha_A^0}\eta_A^2 C_{AA}^{free} + \frac{\alpha_A^0}{\alpha_B^0} C_{6BB}^{eff}} R_{AB}^{-6} \tag{18}$$

The C_{6BB}^{eff} are the effective homonuclear coefficients of the B (MM) atoms. Due to the difficulty to express them through eq 15, in this work their values are parametrized in an atom-type fashion with respect to QM calculations based on the Hirshfeld partitioning proposed in TS.[84,85] α_A^0 and α_B^0 are parametrized with respect to high-level QM calculations (vide infra).

$f_{damp}(R_{AB}, R_A^0, R_B^0)$ in eq 18 is a Fermi-type damping function, which is specified by following the standard approaches exploited to define dispersion corrected density functionals:[43,70,81]

$$f_{damp}(R_{AB}, R_A^0, R_B^0) = \frac{1}{1 + \exp\left[-d\left(\frac{R_{AB}}{s_R R_{AB}^0} - 1\right)\right]} \tag{19}$$

where $R_{AB}^0 = R_A^0 + R_B^0$ and d and s_R are free parameters (see section 5.1).

The dispersion contribution to the QM/MM Fock matrix is

$$F_{\mu\nu}^{dis} = \frac{\partial E_{dis}}{\partial \rho}\frac{\partial \rho}{\partial P_{\mu\nu}} = -\frac{1}{2}\frac{\partial \rho}{\partial P_{\mu\nu}}\sum_{A\in QM}\sum_{B\in MM} f_{damp}(R_{AB})\frac{\partial C_{6AB}}{\partial \rho} R_{AB}^{-6} \tag{20}$$

By considering that the free atomic related quantities are independent of the density matrix, and that the same obviously applies to MM-related quantities, the terms in eq 20 can be written as follows:

$$\frac{\partial C_{6AB}^{eff}}{\partial \rho} = \frac{2\frac{\alpha_A^0}{\alpha_B^0} C_{6BB}^2}{\left(\frac{\alpha_B^0}{\alpha_A^0} C_{6AA}^{eff} + \frac{\alpha_A^0}{\alpha_B^0} C_{6BB}\right)^2}\frac{\partial C_{6AA}^{eff}}{\partial \rho} \tag{21}$$

$$\frac{\partial C_{6AA}^{eff}}{\partial \rho} = C_{6AA}^{free} 2\eta_A \frac{\partial \eta_A}{\partial \rho} \tag{22}$$

$$\frac{\partial \eta_A}{\partial \rho} = \eta_A^\rho = \frac{\int d\mathbf{r}\, r^3 w_A(\mathbf{r})\, \chi_\mu(\mathbf{r})\, \chi_\nu(\mathbf{r})}{\int d\mathbf{r}\, r^3 \rho_A^{free}(\mathbf{r})} \tag{23}$$

where the eff superscript in the C_{6BB} term is omitted for the sake of readability of the equations. In eq 23, the term due to the partial derivative of the density with respect to the density matrix is accounted for. By recollecting all the terms in the above equations, the quantum dispersion contribution to the Fock matrix becomes

$$F_{\mu\nu}^{dis} = -\frac{1}{2}\sum_{A\in QM}\sum_{B\in MM} f_{damp}(R_{AB}) \frac{2\frac{\alpha_A^0}{\alpha_B^0} C_{6BB}^2 C_{6AA}^{free} 2\eta_A}{\left(\frac{\alpha_B^0}{\alpha_A^0} C_{6AA}^{eff} + \frac{\alpha_A^0}{\alpha_B^0} C_{6BB}\right)^2} \eta_A^\rho R_{AB}^{-6} \tag{24}$$

Similarly to the Pauli repulsion term, eq 24 introduces an explicit contribution to the QM Hamiltonian, which propagates to the calculation of molecular properties and spectra, which will be considered in future communications.

3. COUPLING DISPERSION/REPULSION TO NONPOLARIZABLE QM/MM APPROACHES

In electrostatic embedding QM/MM models, the MM atoms are endowed with fixed atomic charges that produce an electric field which polarizes the electron density. The electrostatic embedding introduces a new term in the molecular Hamiltonian, that is, the interaction between the potential generated by the MM charges and the electron density:

$$H_{QM/MM}^{ele} = \sum_{j=1}^{N_{MM}} \int_{\mathbf{R}^3} \frac{\rho_{QM}(\mathbf{r}) q_j}{|\mathbf{r} - \mathbf{r}_j|} d\mathbf{r} \tag{25}$$

In eq 25, the summation runs over the j MM charges. Notice how the MM charges that are parameters of the employed force field are a fundamental quantity: their quality is crucial as they provide a representation, albeit crude, of the electron density of the environment. Quantum Pauli repulsion and quantum dispersion act as additive contributions to eq 25:

DOI: 10.1021/acs.jctc.7b00776
J. Chem. Theory Comput. 2017, 13, 4854−4870

$$
\begin{aligned}
H_{\mathrm{QM/MM}} &= H^{\mathrm{ele}}_{\mathrm{QM/MM}} + H^{\mathrm{rep}}_{\mathrm{QM/MM}} + H^{\mathrm{dis}}_{\mathrm{QM/MM}} \\
&= \sum_{j=1}^{N_{\mathrm{MM}}} \int_{\mathbf{R}^3} \frac{\rho_{\mathrm{QM}}(\mathbf{r}) q_j}{|\mathbf{r} - \mathbf{r}_j|} \mathrm{d}\mathbf{r} \\
&+ \frac{1}{2} \sum_{\mathbf{R}} \int \frac{\mathrm{d}\mathbf{r}_1\, \mathrm{d}\mathbf{r}_2}{r_{12}} \rho_{\mathrm{QM}}(\mathbf{r}_1, \mathbf{r}_2) \\
&[\beta_{\mathbf{R}}^2\, \mathrm{e}^{-\xi_{\mathbf{R}}(\mathbf{r}_1-\mathbf{R})^2} \cdot \mathrm{e}^{-\xi_{\mathbf{R}}(\mathbf{r}_2-\mathbf{R})^2}] + \\
&- \frac{1}{2} \sum_{\mathrm{A}\in\mathrm{QM}} \sum_{\mathrm{B}\in\mathrm{MM}} f_{\mathrm{damp}}(R_{\mathrm{AB}}, R^0_{\mathrm{A}}, R^0_{\mathrm{B}}) \\
&\frac{\eta_{\mathrm{A}}^2 C^{\mathrm{free}}_{\mathrm{AA}} C^{\mathrm{eff}}_{\mathrm{6BB}}}{\frac{\alpha^0_{\mathrm{B}}}{\alpha^0_{\mathrm{A}}} \eta_{\mathrm{A}}^2 C^{free}_{AA} + \frac{\alpha^0_{\mathrm{A}}}{\alpha^0_{\mathrm{B}}} C^{\mathrm{eff}}_{\mathrm{6BB}}} R_{\mathrm{AB}}^{-6}
\end{aligned}
\tag{26}
$$

By expanding ρ_{QM} in a finite basis set $\{\chi_\mu\}$ and taking the derivative with respect to the density matrix $P_{\mu\nu}$, it is possible to define the contribution to the Fock matrix:

$$
\begin{aligned}
F_{\mu\nu} &= h_{\mu\nu} + G_{\mu\nu}(\mathbf{P}) + \mathbf{V}^{\dagger}_{\mu\nu}\mathbf{q} \\
&+ \frac{1}{2} \int \mathrm{d}\mathbf{r}_1 \left[\frac{\chi_\mu(\mathbf{r}_1)\, A_\nu(\mathbf{r}_1) + A_\mu(\mathbf{r}_1)\, \chi_\nu(\mathbf{r}_1)}{2} \right] + \\
&- \frac{1}{2} \sum_{\mathrm{A}\in\mathrm{QM}} \sum_{\mathrm{B}\in\mathrm{MM}} f_{\mathrm{damp}}(R_{\mathrm{AB}}) \\
&\frac{2\frac{\alpha^0_{\mathrm{A}}}{\alpha^0_{\mathrm{B}}} C^2_{\mathrm{6BB}} C^{\mathrm{free}}_{\mathrm{6AA}} 2\eta_A}{\left(\frac{\alpha^0_{\mathrm{B}}}{\alpha^0_{\mathrm{A}}} C^{\mathrm{eff}}_{\mathrm{6AA}} + \frac{\alpha^0_{\mathrm{A}}}{\alpha^0_{\mathrm{B}}} C_{\mathrm{6BB}}\right)^2} \eta^{\rho}_{\mathrm{A}} R_{\mathrm{AB}}^{-6}
\end{aligned}
\tag{27}
$$

3.1. Coupling Dispersion/Repulsion to the Polarizable QM/FQ Model. In polarizable embedding QM/MM models, the mutual polarization of the MM and QM portions is explicitly taken into account. The MM force field contains a *response* term, which modifies the electrostatics as a reaction to the presence of the QM density. In a symmetric fashion, a polarization term is included in the core's Hamiltonian to represent the interaction of the electronic density with the MM electrostatics. If the polarizability of the MM region is introduced by means of induced point dipoles,[31,32,86] the electric field produced by the QM density appears in the equations that determine the dipoles, and the dipoles appear in an interaction term in the Hamiltonian multiplied by a field operator. If instead a fluctuating charge (FQ) description[26,27,49,87,88] is adopted to make the force field polarizable, the electrostatic potential produced by the QM density gives rise to a charge flow in the MM region; the MM fluctuating charges in turn interact with the QM density. Therefore, the expression for the interaction between the QM and MM portions is the same as eq 25, but the charges are in this case calculated by solving the following response equation:[47]

$$
\mathbf{D}\mathbf{q}_\lambda = -\mathbf{C}_{\mathrm{Q}} - \mathbf{V}(\mathbf{P}_{\mathrm{QM}}) \tag{28}
$$

where $\mathbf{D}$ is the response matrix whose diagonal terms are the atomic electronegativities, $\mathbf{q}$ is a vector containing the FQs and the Lagrangian multipliers, $\mathbf{C}$ is a vector containing the atomic electronegativities and the constraints to ensure that each MM molecule has fixed charge, and $\mathbf{V}(\mathbf{P})$ is the potential due to the QM density matrix $\mathbf{P}$. The Pauli repulsion and quantum dispersion terms developed in the previous pages can be added to the QM/FQ Hamiltonian in the same fashion as in eq 26. The resulting expression is the same; however the q_j charges in eq 26 and eq 27 this time are the FQs calculated through eq 28 at each step of the SCF procedure.

4. COMPUTATIONAL DETAILS

The equations presented in the previous section were implemented in the Gaussian 16 computational package.[89] Notice that the current implementation of eq 9 is restricted to uncontracted basis sets of s-, p-, and Cartesian d-type primitive Gaussian functions. All QM/FQ and QM/nonpolarizable MM calculations were performed by treating the QM portion at the DFT level of theory, combined with selected Pople-type basis sets. The parameters to treat the electrostatic component in FQ calculations were taken from Rick et al.[26] The TIP3P[90] force field was exploited in nonpolarizable MM calculations. All the classical molecular dynamics (MD) simulations were performed by using the Gromacs package,[91−94] with the same settings as previously reported by some of the present authors.[13,95] The Kitaura−Morokuma energy decomposition analysis (KM-EDA)[96,97] was performed by using the GAMESS package.[98,99] Symmetry adapted perturbation theory (SAPT)[41,42] calculations were performed by using Psi4 1.1.[100]

5. NUMERICAL RESULTS

In this section, the methodology explained in sections 2 and 3 is applied to test cases. In particular, the model is first parametrized to treat the aqueous solution, so to reliably reproduce some of the most relevant properties of bulk water. Then, the method is applied to the calculation of the nonelectrostatic interaction energy of molecular systems in aqueous solution.

5.1. Parametrization Strategy: Aqueous Solutions. The methodology stretched in the previous sections is general enough to be applied to different polarizable and nonpolarizable QM/MM approaches and to model any kind of external environment, pending an appropriate parametrization of the quantities entering eqs 11, 12, 18, and 24. Such a parametrization is a crucial step toward the routinely application of the method to real cases. The development of accurate parametrizations for various kinds of environments is beyond the scope of this paper. Here, we will present the strategy that is followed to parametrize the method coupled with our polarizable QM/MM model based on FQs (QM/FQ) and specifically tailored to aqueous solutions.[13,24,47,101]

In the specific case of water, eq 4 requires the definition and the numerical setting of four parameters: the exponents of the lone pairs and bond pairs $\beta_{\mathbf{R}}$ and the coefficients $\xi_{\mathbf{R}}$. In fact, the use of the same parameters for bond and lone pairs would not been justified. Also, the actual positions of the Gaussian-type functions (eq 3) has to be set, and this introduces a further degree of freedom in the parametrization procedure. In the case of water, eq 3 reads:

$$
\rho_{\mathrm{H_2O}}(\mathbf{r}_1, \mathbf{r}_2) = \sum_{j=1}^{N_{\mathrm{H_2O}}} \sum_{i=1}^{4} \xi_i^2\, \mathrm{e}^{-\beta_i(\mathbf{r}_1-\mathbf{R}_i^{(j)})^2}\, \mathrm{e}^{-\beta_i(\mathbf{r}_2-\mathbf{R}_i^{(j)})^2} \tag{29}
$$

where j runs over the water molecules of the MM portion, while i runs over the electron pairs of a single water molecule. Two sets of indices β_i and ξ_i are set, and again they differ if a lone pair or a bond pair is considered. $\mathbf{R}_i^{(j)}$ collects the points where the Gaussian-type functions are centered, which are chosen in analogy with what is done in the TIP4P force field.[102] In particular, the $\mathbf{R}_i^{(j)}$ centers are set as the charge centroids of the localized molecular orbitals, as defined according to the Boys

DOI: 10.1021/acs.jctc.7b00776
J. Chem. Theory Comput. 2017, 13, 4854−4870

method[103] (see Figure 1), which in the present case were calculated at the B3LYP/6-311++G** level of theory (see section S2 in SI).

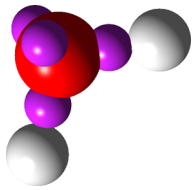

Figure 1. Calculated B3LYP/6-311++G** Boys localized orbitals centroids (purple spheres) for a single water molecule.

Notice that the way the ρ_{MM} is constructed permits extension of this approach to solvents/environments other than water. Also, in the present work ρ_{MM} is defined in terms of spherical Gaussian-type functions only.

By further substituting eq 29 in eq 2, we obtain

$$E^{rep}_{QM/H_2O} = \frac{1}{2}\sum_{j=1}^{N_{H_2O}}\sum_{i=1}^{4}\int \frac{d\mathbf{r}_1 d\mathbf{r}_2}{r_{12}} \rho_{QM}(\mathbf{r}_1, \mathbf{r}_2)\left[\xi_i^2\, e^{-\beta_i(\mathbf{r}_1-\mathbf{R}_i^{(j)})^2}\, e^{-\beta_i(\mathbf{r}_2-\mathbf{R}_i^{(j)})^2}\right] \quad (30)$$

In order to set the parameters entering eq 30, selected water clusters, chosen by following refs 104 and 105 (see Figure 2),

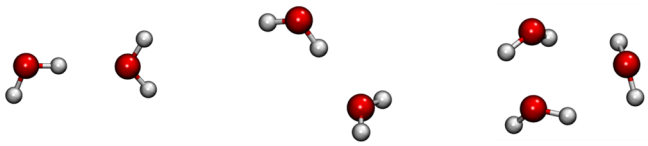

Figure 2. Water clusters used for the parametrization of E^{rep}_{QM/H_2O}, see text.

were exploited. In particular, the reference full QM data for the Pauli repulsion energy of such clusters were calculated by performing a full QM calculation on each structure in Figure 2 at the Hartree–Fock (HF) level in combination with selected Pople-type basis sets, also including diffuse functions (6-31G, 6-31+G*, 6-311G, 6-311+G*). Then, the repulsion contribution to the energy was extracted by resorting to the KM-EDA,[96,97] by following what has already been proposed in the literature.[104,105]

Then, the Pauli Repulsion on the same water clusters was calculated with our method (eq 30). This has been done by treating only one water molecule at the QM level (B3LYP functional combined with the same selection of basis sets) and the other one (or two, in case of the trimer in Figure 2) at the FQ level. For each dimer structure, we performed two calculations, by exchanging the QM and FQ water molecules in order to average among hydrogen bond donor and acceptor moieties. Three calculations were performed for the trimer, by exchanging each time the QM molecule with one of the two FQ molecules.

Eq 30 depends on four parameters (the exponents and the coefficients of each Gaussian function): their best values were defined by performing a least-square-root's fitting on full QM data obtained with the KM-EDA approach, without setting any constraint on the parameters. The best fitted values are reported in section S2 in the SI. Notice that such values give repulsion energies not perfectly fitting the KM-EDA data (see Table S1 in the SI); this is probably due to the absence of the contributions due to p-type Gaussian functions in the MM moiety. Such functions can possibly be added by extending the formalism in a straightforward way, by only making the computations more cumbersome.

Moving to quantum dispersion (eq 18), its expression depends on several parameters, which were set according to the following scheme:

- α_0 are static atomic polarizabilities. They were calculated at the CCSD(T)/aug-cc-pVTZ level of theory, or taken from the literature.[106] The used values are reported in Table S2, in the SI.
- The homonuclear C_6^{free} coefficients were taken from Chu and Dalgarno[107,108] and are reported in Table S3 in the SI.
- The homunuclear C_6^{eff} coefficients of the MM atoms cannot be intuitively defined, because they actually depend on the effective volume of a given atom in a molecule. Since our target environment is water, the effective volumes of oxygen and hydrogen atoms in a water molecule optimized at the B3LYP/6-311++G** level were calculated. From these values, the C^{eff}_{6OO} and C^{eff}_{6HH} were calculated, being 14.8 hartree·bohr^6 and 2.8 hartree·bohr^6, respectively. Notice that these data are in agreement with those proposed by TS.[43]
- The d coefficient of eq 19 was set to 20, according to the TS approach.[43] An extensive testing was however performed, showing that similar E_{dis} values are obtained for any choice of d between 15 and 40.
- The van der Waals radii R^0 were set to the Bondi reference values.[109]
- As previously noticed in the literature,[43] the s_R coefficient in eq 19 is actually the only empirical parameter. s_R was chosen in such a way that E_{dis} of a water dimer as a function of the intermolecular distance O–O (calculated at the B3LYP-D3 level of theory) is accurately reproduced. The s_R coefficient was therefore set to 0.92, which gives an average error of about 5% in the region of hydrogen bonding (d_{O-O} 2.5–3.0 Å; see below for more details). Notice that the calculated E_{dis} at the equilibrium distance between two neighbor water molecules (d_{O-O} = 2.9 Å)[110] is very close to the value reported recently by Guidez and Gordon.[111]

5.2. Dependence of E_{rep} and E_{dis} on the Water–Water Intermolecular Distance. In this section, the dependence of E_{rep} and E_{dis} on the water–water intermolecular distance is studied. To this end, the water dimer depicted in Figure 3 has

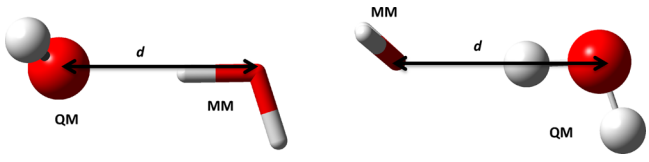

Figure 3. Structure of the water dimer used to study the dependence of E_{Qnel} on the water–water intermolecular distance.

been exploited, and the distance d between the oxygen atoms has been taken as a reference. Notice that this distance has been chosen as reference because it is generally reported in the experimental/computational evaluation of radial distribution functions.[110]

In Figure 4, E_{rep} is reported as a function of d. The plot was constructed by performing 80 calculations increasing the O–O distance from 2.54 to 6.49 Å by a step of 0.05 Å. E_{rep} was calculated both with the QM/FQ and nonpolarizable QM/MM(TIP3P) methods, by exploiting the B3LYP/6-31+G* level to treat the QM moiety. Also in this case, the QM and MM

DOI: 10.1021/acs.jctc.7b00776
J. Chem. Theory Comput. 2017, 13, 4854–4870

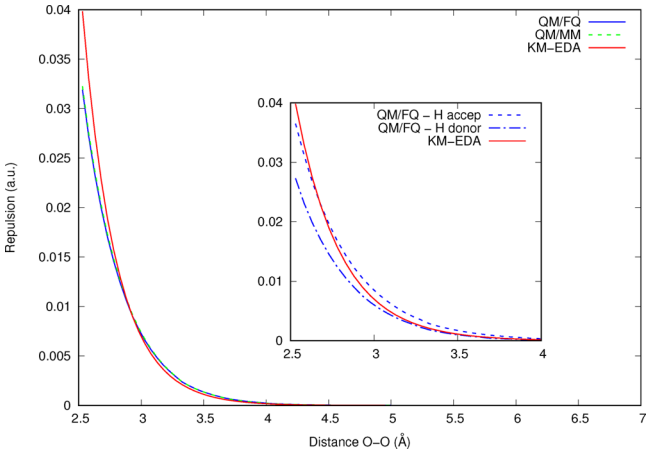

Figure 4. Plot of E_{rep} as a function of the O−O intermolecular distance in the water dimer depicted in Figure 3. QM/FQ and nonpolarizable QM/MM(TIP3P) values (B3LYP/6-31+G* for the QM moiety) are compared to KM-EDA (HF/6-31+G*) calculations. The inset shows E_{rep} calculated values with the QM/FQ approach, in case the QM water molecule acts as an H-bond donor or acceptor.

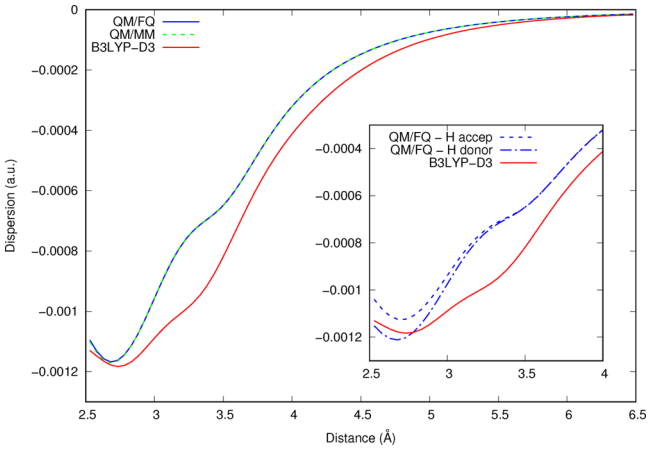

Figure 5. QM/FQ and nonpolarizable QM/TIP3P (B3LYP/6-31+G* for the QM moieties) quantum dispersion energy, E_{dis}, of the water dimer in Figure 3 as a function of the O−O distance. B3LYP-D3/6-31+G* data are also reported. The inset shows E_{dis} calculated values with the QM/FQ approach, in case the QM water molecule acts as a H-bond donor or acceptor.

moieties were interchanged, and the average values were taken. In Figure 4, these data are compared with the repulsion energy obtained at the full QM level by means of the KM-EDA approach.

An almost perfect superposition of QM/FQ and QM/MM results is observed. For d < 3.5 Å, for which E_{rep} is large, the QM/FQ method shows an average percentage deviation from the full QM KM-EDA of around 10%, similarly to the nonpolarizable QM/TIP3P approach. Notice that the QM/FQ results are in very good agreement with KM-EDA results in the region around d = 3 Å. This is not unexpected, because the water−water structures that were exploited to perform the parametrization of this contribution (see Figure 2) were characterized by a similar intermolecular distance (2.04 Å).

The inset in Figure 4 shows in more detail the difference between the calculated QM/FQ and KM-EDA values in the region between 2.5 and 4 Å; the two curves obtained for the QM water molecule acting as H-bond donor and acceptor are given. We notice that E_{rep} is larger when the QM water molecule acts as a H-bond acceptor. This is due to the fact that the Gaussian function in eq 29 on the MM O−H water bond is larger than that related to the fictitious MM oxygen atom lone pair (i.e., the exponent of the function placed in the middle of the O−H distance is smaller than the exponent of the function placed at the position of the fictitious O lone pair). Therefore, the overlap between the Gaussian functions and the QM density is larger when the MM water molecule acts as a H-bond donor, and this corresponds to a greater value of E_{rep}. The inset in Figure 4 also shows that the KM-EDA values lie almost always in between the two QM/FQ curves. This supports the averaging of the two values in the parametrization procedure (see the previous section). At small intermolecular distances the repulsion contribution is underestimated. This is probably related again to the absence of p-type Gaussian functions on the MM moiety, which would guarantee a greater overlap of the QM and MM densities.

Let us pass to discuss the dependence of the E_{dis} as a function of the intermolecular O−O distance. The data are plotted in Figure 5, which also reports the curve obtained with the B3LYP-D3 functional.[81]

Notice that also in this case the QM and MM moieties were interchanged (see inset in Figure 5). Different from E_{rep}, E_{dis} is larger (in absolute value) when the QM water molecule acts as a H-bond donor. This can be explained by considering the values obtained for the effective C_6^{eff} coefficients for the MM molecule (see previous section). In fact, when the QM molecule acts as a H-bond donor, the oxygen atom of the MM water molecule is close to the QM portion; because C_{6OO}^{eff} is greater than C_{6HH}^{eff} (14.8 vs 2.8 hartree·bohr^6), E_{dis} increases.

The behavior of the total quantum nonelectrostatic interaction energy E_{Qnel}, i.e., the sum of E_{rep} and E_{dis}, as a function of d is plotted in Figure 6, which also reports the SAPT2 + 3(CCD)/aug-cc-pVDZ curve. Also in this case the QM and MM moieties were interchanged (see inset in Figure 6). Comparison of Figures 5 and 4 shows that the repulsion term is generally larger than the dispersion contribution: this clearly emerges from the trend reported in Figure 6, which closely resembles Figure 4. It is also

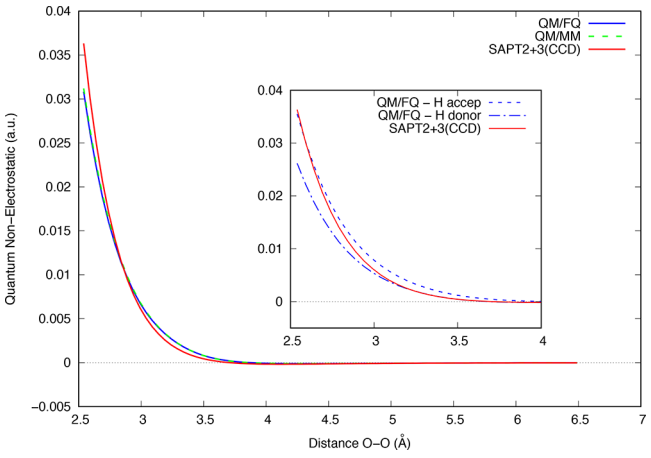

Figure 6. QM/FQ and nonpolarizable QM/TIP3P (B3LYP/6-31+G* for the QM moieties) quantum nonelectrostatic interaction energy, E_{Qnel}, of the water dimer in Figure 3 as a function of the O−O distance. SAPT2 + 3(CCD)/aug-cc-pVDZ data are also reported. The inset shows E_{Qnel} calculated values with the QM/FQ approach, in case the QM water molecule acts as a H-bond donor or acceptor.

DOI: 10.1021/acs.jctc.7b00776
J. Chem. Theory Comput. 2017, 13, 4854−4870

worth pointing out that QM/FQ and nonpolarizable QM/TIP3P give similar E_{Qnel} values. This is a further evidence of the stability of our parametrization, which gives similar results as changing the force field used to represent the MM portion.

To end this discussion, the total interaction energy as a function of d is plotted in Figure 7 and compared with

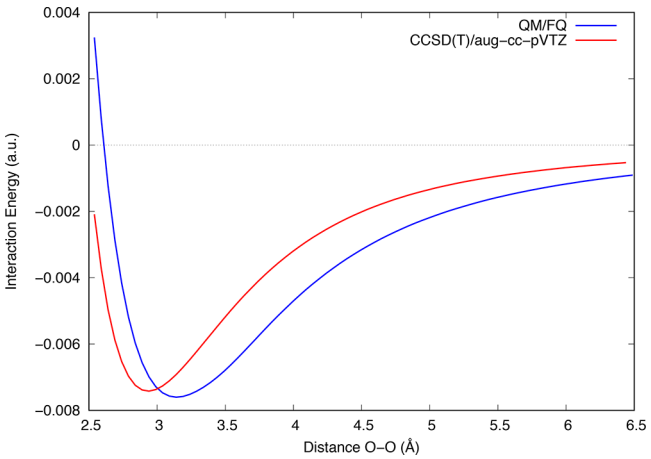

Figure 7. QM/FQ (B3LYP/6-31+G* for the QM moieties) and CCSD(T)/aug-cc-pVDZ total interaction energy for the water dimer in Figure 3 as a function of the O−O distance.

CCSD(T)/aug-cc-pVTZ data (counterpoise corrections are included). The differences in the two curves can be attributed to the electrostatic contributions and the lack in our model of charge transfer effects and multipole terms. The equilibrium distance is a bit shifted in our model (3.14 Å vs 2.99 Å), but the interaction energy at the equilibrium distance is accurately reproduced with an error of only 7% with respect to the CCSD(T) data and comparable with similar data reported in the literature.[111−113]

5.3. Testing on Water Dimers. In order to test the quality of the parametrization presented in the previous sections, the methodology was applied to ten water dimer structures, taken from Kratz and co-workers (see Figure 8).[114]

All the calculations were performed with both the QM/FQ and QM/MM(TIP3P) methods, coupled with the B3LYP/6-31+G* level for the QM moiety. Again, each time the QM and

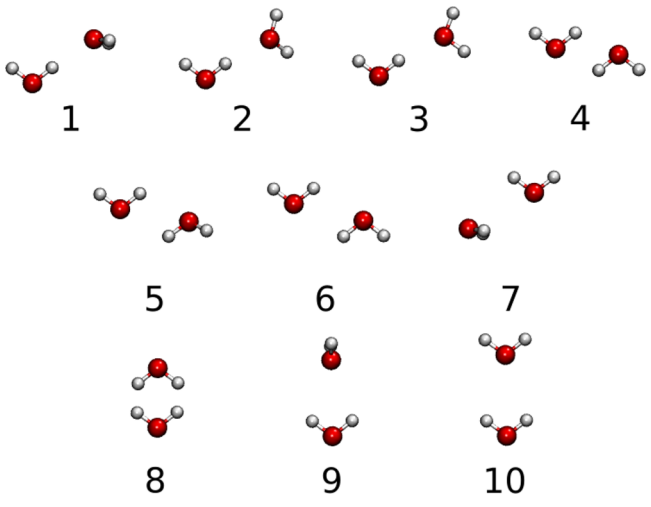

Figure 8. Selected water dimer structures, taken from Kratz et al.[114]

MM portions were exchanged, and the two values averaged to get the final results (see previous section). E_{rep} values were compared to KM-EDA data (see Figure 9 and Table 1). QM/FQ and QM/

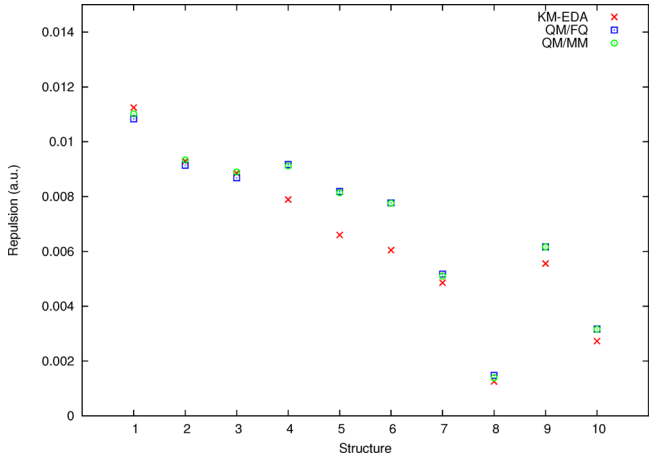

Figure 9. Calculated QM/FQ and QM/TIP3P (B3LYP/6-31+G*) E_{rep} values for the water dimer structures in Figure 8. KM-EDA (HF/6-31+G*) data are also reported for comparison.

Table 1. Calculated E_{rep} (10^{-3} Hartree) for the 10 Water Dimers[a]

	KM-EDA	QM/FQ	Δ	Err %	QM/TIP3P	Δ	Err %
1	11.245	10.831	1.517	3.68	11.013	0.550	2.06
2	9.284	9.138	1.203	1.57	9.334	0.320	0.54
3	8.856	8.687	1.154	1.91	8.897	0.285	0.46
4	7.892	9.167		16.16	9.118		15.54
5	6.600	8.185	0.003	24.02	8.139	0.001	23.32
6	6.046	7.769		28.51	7.756		28.28
7	4.858	5.174	0.039	6.51	5.100	0.516	4.99
8	1.255	1.478		17.75	1.391		10.81
9	5.556	6.161	1.506	10.89	6.164	1.159	10.94
10	2.727	3.168	0.738	16.17	3.162	0.533	15.95
average error				12.72			11.29

[a]Δ shows the deviation obtained by exchanging the QM and MM moieties. The percentage error from the KM-EDA values is also reported.

TIP3P values are very similar, although the parametrization has been performed only with the QM/FQ method, thus confirming once again the stability of our approach. The largest deviation from KM-EDA results is given by structures 4−6, which show the smallest oxygen−oxygen distance, probably due to the absence of p-type Gaussian functions placed at lone pair positions.

The Δ values in Table 1, i.e. the half-difference of the two calculations performed by exchanging the QM and MM moieties, are larger for structures characterized by a strong H−O intermolecular interaction. Furthermore, except for structure 7, the QM/FQ Δ values are greater than the corresponding QM/MM ones. This difference is linked to the different physical description of the MM portion in the polarizable and nonpolarizable models. In fact, the polarizable QM/FQ approach emphasizes the H-bond acceptor or donor characters of the MM molecule, thus resulting in a different interaction with the QM densities.

The total calculated quantum nonelectrostatic contribution (E_{Qnel},i.e. the sum of the Pauli repulsion and quantum

DOI: 10.1021/acs.jctc.7b00776
J. Chem. Theory Comput. 2017, 13, 4854−4870

dispersion) is reported in Table 2. Only QM/FQ data are shown, due to the similarity of the calculated results by exploiting the

Table 2. E_{rep}, E_{dis}, E_{Qnel}, Electrostatic Energies (E_{FQs}), and Total Interaction Energies, E_{tot}, for the 10 Water Dimers[a]

	E_{rep}	E_{dis}	E_{Qnel}	E_{FQ}	E_{tot}
1	10.831	−1.123	9.708 (34%)	−18.483 (66%)	−8.775
2	9.138	−1.005	8.133 (33%)	−16.823 (67%)	−8.690
3	8.687	−0.977	7.710 (31%)	−17.014 (69%)	−9.304
4	9.167	−1.005	8.162 (35%)	−15.190 (65%)	−7.028
5	8.185	−0.988	7.197 (33%)	−14.516 (67%)	−7.319
6	7.769	−0.986	6.783 (31%)	−14.852 (69%)	−8.069
7	5.174	−1.687	3.487 (24%)	−11.068 (76%)	−7.581
8	1.478	−1.046	0.432 (12%)	−3.169 (88%)	−2.737
9	6.161	−1.174	4.987 (29%)	−12.498 (71%)	−7.511
10	3.168	−1.119	2.049 (18%)	−9.409 (82%)	−7.360

[a]The values in parentheses give the percentage of the corresponding contribution with respect to E_{tot}. All energy values are given in 10^{-3} Hartree.

QM/FQ and QM/TIP3P approaches. According to what is expected for aqueous solutions, which are dominated by electrostatic interaction, E_{Qnel} is always smaller than the electrostatic term (E_{FQ}). However, the London contribution is not negligible, being as large as 35% of the total interaction energy.

A closer look at Table 2 shows that E_{Qnel} is generally dominated by the Pauli repulsion interaction, which is always larger than E_{dis}. This behavior confirms the results reported above, where the dependence of such contributions on the intermolecular distance was outlined. Furthermore, the two terms are very similar for some structures, such as 8 and 10, thus demonstrating that the inclusion of both terms is compulsory to get a reliable description of E_{Qnel}.

To end the discussion on these water dimers, in Table 3 the total Quantum non electrostatic calculated by our approach is compared with SAPT2 + 3(CCD)/aug-cc-pVDZ values.

Table 3. E_{Qnel} for the 10 Water Dimers Calculated by Using Our Model and the SAPT2 + 3(CCD)/aug-cc-pVDZ[a]

	E_{Qnel}(QM/FQ)	E_{Qnel}(SAPT)
1	9.708 (1%)	9.814
2	8.133 (3%)	7.882
3	7.710 (3%)	7.451
4	8.162 (19%)	6.863
5	7.197 (35%)	5.348
6	6.783 (44%)	4.707
7	3.487 (20%)	4.381
8	0.432 (50%)	0.866
9	4.987 (6%)	4.693
10	2.049 (2%)	2.000

[a]The values in parentheses give the percentage of the corresponding contribution with respect to the last column. All energy values are given in 10^{-3} Hartree.

As already pointed out, the largest deviation from SAPT values is given by structures 4−6, which show the smallest oxygen−oxygen distance. Notice that the largest error is shown by dimer 8, for which, however, E_{Qnel} is very small and the deviation in absolute value is even smaller than for the other structures.

To further testing the quality of our approach, the model is applied to the water dimer in Figure 10, previously studied by Guidez and Gordon[111] by exploiting the EFP2(E_6 + E_7) model.

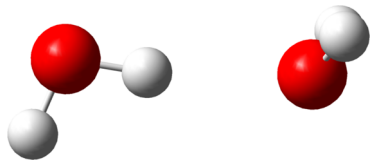

Figure 10. Structure of the water dimer optimized at the MP2/aug-cc-pVDZ level of theory[115] previously studied by Guidez and Gordon.[111]

In Table 4, the three terms entering in the definition of the interaction energy are reported as calculated by our model, the

Table 4. Electrostatic, Exchange-Repulsion, Dispersion and Total Interaction Energy for the Water Dimer Depicted in Figure 10 Calculated by Using Our Model, EFP2(E_6 + E_7)[111] and Energy Decomposition Analysis EDA (CCSD(T)/aug-cc-pVQZ//MP2/aug-cc-pVQZ)[112][a]

level of theory	QM/FQ	EFP2(E_6 + E_7)[111]	EDA[112]
electrostatic[b]	−11.01 (2%)	−9.32 (14%)	−10.79
exchange repulsion	6.57 (8%)	5.59 (22%)	7.16
dispersion	−0.70 (47%)	−0.51 (62%)	−1.33
charge transfer	N/A	−0.47	N/A
total interaction energy	−5.15(4%)	−4.71 (5%)	−4.95

[a]The values in parentheses give percentages with respect to the values in the last column. All energy values are given in kcal/mol. [b]For EFP2 and EDA the electrostatic term is the sum of Coulomb and polarization contributions.

EFP2(E_6 + E_7) and the Energy Decomposition Analysis performed at CCSD(T)/aug-cc-pVQZ level of theory, with the further inclusion of counterpoise corrections.

In the QM/FQ approach, electrostatic and polarization contribution cannot be separated, as previously reported by some of the present authors.[47] Therefore, a single term is reported in Table 4. The largest deviation with respect to the EDA is shown by the dispersion term. However, as pointed out by Guidez and Gordon,[111] EDA overestimates the dispersion interaction due to the fact that it is computed as the difference between CCSD(T) and HF interaction energies. Overall, the agreement between our data and EDA is satisfactory, being the errors for the single terms generally small and the total interaction energy similar to the EDA value.

5.4. Dependence of E_{rep} and E_{dis} on the QM Description. In this section, the dependence of calculated E_{rep} and E_{dis} values on the level used to model the QM moiety is studied. To this end, the water dimer depicted in Figure 3 with d = 2.64 Å is exploited. Eight different DFT functionals were selected, by following the recent literature,[116,117] ranging from pure (B97D[118,119]), to different classes of hybrid functionals (B3LYP,[120] B3PW91,[121] M062X,[122] PBE0,[123] SOGGA11-X[124]), also including long-range (CAM-B3LYP[125]) and dispersion corrections (ωB97xD[126]). Each functional was coupled to several Pople-type basis sets (see Figure 11 and Figure 12), in order to separate the contribution arising from polarization and diffuse functions.

Figure 11 reports schematically the trends obtained by computing E_{rep} with the different DFT functionals and the different basis sets. Numerical values are given in Table S4 in the

DOI: 10.1021/acs.jctc.7b00776
J. Chem. Theory Comput. 2017, 13, 4854−4870

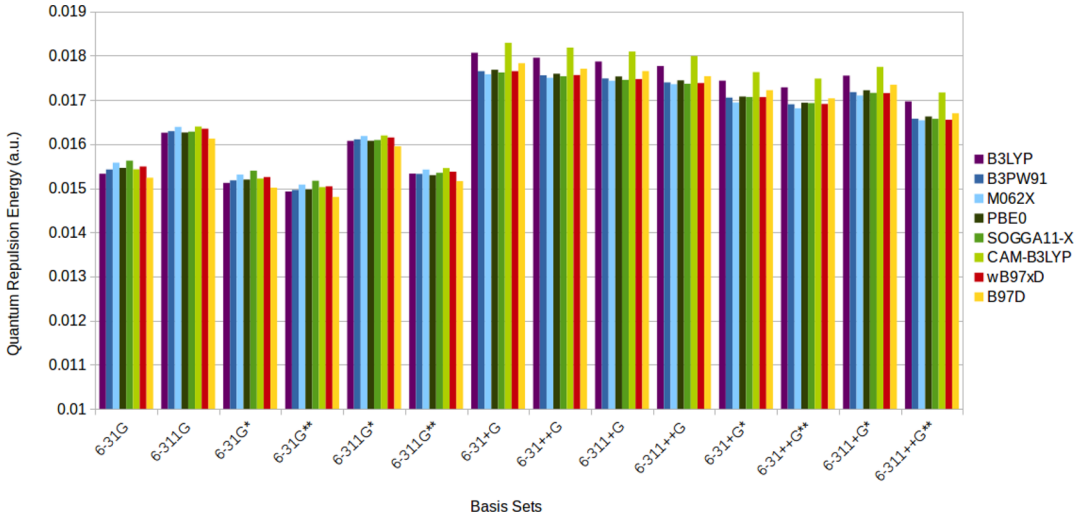

Figure 11. Dependence of E_{rep} on the basis set and DFT functional for the water dimer depicted in Figure 3.

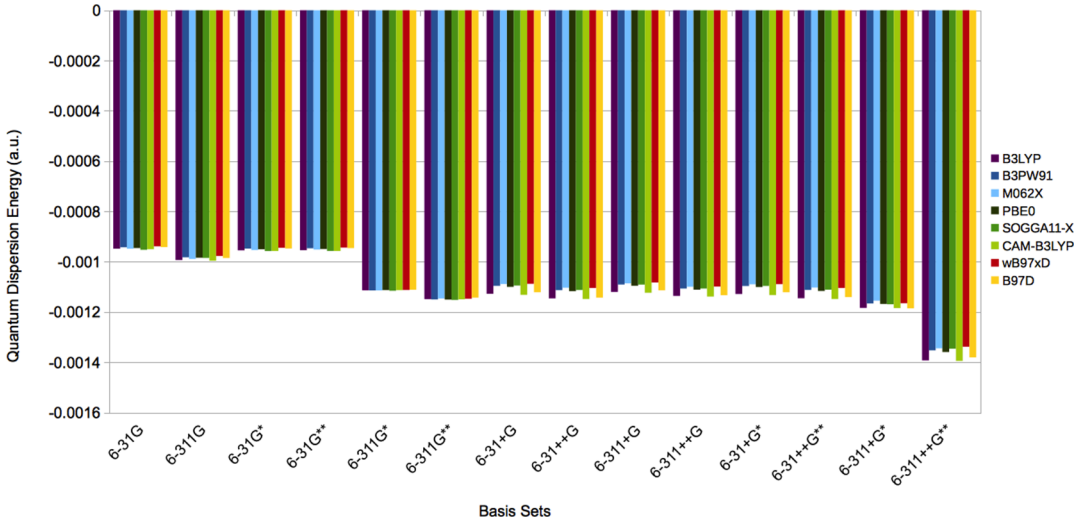

Figure 12. Dependence of E_{dis} on the basis set and DFT functional for the water dimer depicted in Figure 3.

SI. All DFT functionals predict very similar E_{rep} values as varying the basis set, with CAM-B3LYP always showing the highest values for a given basis set (on average, the CAM-B3LYP values are about 2% higher than the average value of the other functionals). This is not surprising, if the tendency of the CAM-B3LYP of spreading out the QM density is considered. Thus, the overlap between the QM density and the MM one is enlarged, resulting in an increase of E_{rep}.

The reported dependence on the choice of the basis set is also not surprising. In fact, the addition of functions on the hydrogen atoms (e.g., from 6 to 31G to 6-311G) increases the QM-MM overlap, and E_{rep} increases of about 6% on average. Such an increase is reduced when diffuse functions are included. The effect of polarization functions is usually negligible, however the addition of such functions generally results in the decreasing of E_{rep}, especially moving from single to double polarization functions. The addition of diffuse functions causes instead an increase of E_{rep}, due to an enlarged overlap between the QM and MM densities.

Figure 12 reports the same analysis applied to E_{dis} (raw data are given in Table S5 in the SI).

The results reported in Figure 12 show some general trends, that are very similar to what already observed for E_{rep}. First, CAM-B3LYP predicts the highest E_{dis}, and again this is probably due to the peculiarities of this functional. The observed trend as varying the basis set is similar to what has already been commented for E_{rep}. In fact, the addition of functions on hydrogen atoms increases E_{dis} of about 8%, and this increment is reduced when diffuse functions are considered. Once again, the effect of polarization functions is negligible, and finally results in the decreasing of E_{dis}, especially when double polarization functions are included. An opposite effect is observed when diffuse functions are added: an increase of E_{dis} is noticed, due to larger effective volumes of QM atoms and C_6^{eff} coefficients (see eq 15).

The global effect of the choice of the DFT functional and basis set on E_{Qnel} is reported in Figure S3 in the SI (raw data are given in Table S6 in the SI). To end this discussion, it is worth pointing out that the results of the model here proposed are very stable as the functional and basis set vary. Furthermore, stable values of E_{rep} and E_{dis} are obtained by adding diffuse functions, so that their inclusion appears mandatory. For this reason, in the following

DOI: 10.1021/acs.jctc.7b00776
J. Chem. Theory Comput. 2017, 13, 4854−4870

section the 6-31+G* basis set, which adequately reproduces the total E_{Qnel}, is exploited.

6. MOLECULAR SYSTEMS IN AQUEOUS SOLUTION DESCRIBED WITH THE QM/FQ APPROACH

We have shown in the previous section that our model permits a correct reproduction of the properties of the aqueous solution. In this section we will focus on the calculation of the non-electrostatic contribution to the energetic properties of molecular systems in bulk aqueous solution, as modeled with the QM/FQ approach. We first notice that only the closest FQ solvent molecules will reasonably give a not negligible contribution to the solute−solvent interaction energy, due to the short-range character of E_{rep} and E_{dis}. This feature can help at reducing the computational cost of the calculation. In fact, suitable thresholds can be set. For quantum dispersion (eq 18) a cutoff is set, so that this term vanishes at intermolecular distances larger than 10 Å. Notice however that the further consideration of larger solvent shells would not increase much the computational demand.

On the contrary, the computational cost of the quantum repulsion term (eq 4) strongly depends on the number of water molecules around the solute, because each of them bears the Gaussian functions used to represent ρ_{MM}; increasing the number of Gaussian functions, makes the calculation of the two-electron integral in eq 4 more and more cumbersome. Thus, the setting of a threshold appears beneficial.

To this end, only those FQ water molecules having a geometric center closer to at least a QM atom than a given geometric parameter R are included in the calculation of E_{rep}. In the practice, this requires to build up a cavity made of the union of identical spheres centered on each QM atom: only the MM molecules lying inside this cavity are considered in the evaluation of E_{rep}. Notice that in the present implementation the same radius R is used for different QM atom types: this may be possibly refined.

In order to validate this approach and to set a reasonable value of R, we took as test cases two random snapshots taken from a MD simulation of (L)-Methyl Lactate (MLAT) and (R)-Methyloxirane (MOXY) in aqueous solution. MOXY is a small rigid almost spherical molecule, whereas MLAT develops in the plane of the sp^2 carbon atom. On such snapshots, E_{rep} was calculated as a function of R by using the B3LYP/6-31+G* level to treat the QM solute. The results of such calculations are reported in Figure 13 for the resulting systems depicted in Figure 14 and 15. Notice that such figures only show the FQ water molecules relevant for the evaluation of E_{rep}, i.e. those within a range of variation of R between 1.5 and 5 Å with a step of 0.5. The other FQ water molecules are indeed present, but only contribute to the electrostatic interaction. The numbers of relevant water molecules associated at each radius for the structures depicted in Figure 14 and 15 are reported in Table 5.

Figure 13 clearly shows that the trend of E_{rep} as a function of R strictly depends on the studied system. Also, the structure of the resulting clusters for a given R differs for the two systems. MLAT has a greater surface area and a larger number of H-bond sites with respect to MOXY. This implies a greater exchange repulsion energy contribution for MLAT than for MOXY. Convergence in the repulsion energy value is reached at different values of the atomic radius R. In particular, imposing R = 3.5 Å is sufficient to describe the repulsion contribution for MOXY, whereas for MLAT a slightly larger value (R = 4 Å) is required. This is connected to the relative atomic positions: in case of MOXY,

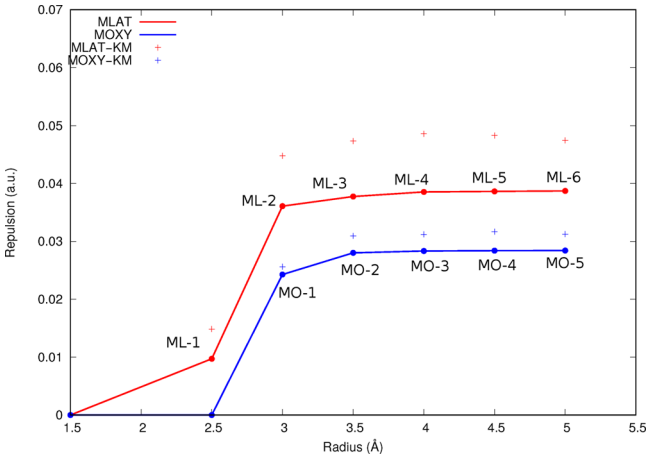

Figure 13. E_{rep} of (L)-methyl lactate and (R)-methyloxirane in aqueous solution as a function of R. B3LYP/6-31+G* is used to treat the QM solute. E_{rep} calculated by exploiting the KM-EDA approach, at the HF/6-31+G* level of theory, is also reported.

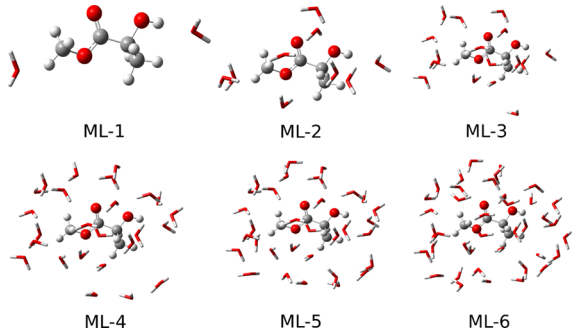

Figure 14. (L)-methyl lactate−water clusters arising from different choices of R.

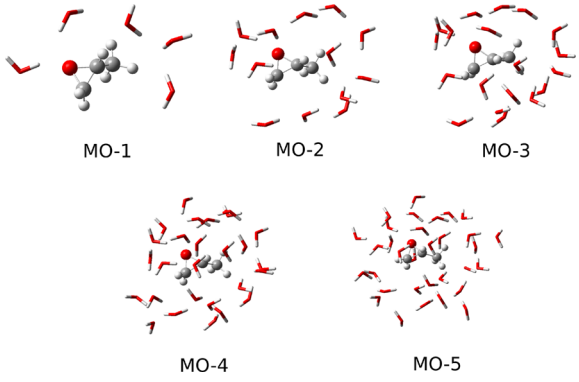

Figure 15. (R)-methyloxirane−water clusters arising from different choices of R.

Table 5. Radii (Å) of the Spheres Centered in Each QM Atom, and Total Number of Relevant Water Molecules for the Structures Depicted in Figures 14 and 15

structure	radius	N_{wat}	structure	radius	N_{wat}
ML-1	2.5	2	MO-1	3.0	5
ML-2	3.0	9	MO-2	3.5	13
ML-3	3.5	16	MO-3	4.0	19
ML-4	4.0	25	MO-4	4.5	27
ML-5	4.5	32	MO-5	5.0	32
ML-6	5.0	39			

DOI: 10.1021/acs.jctc.7b00776
J. Chem. Theory Comput. 2017, 13, 4854−4870

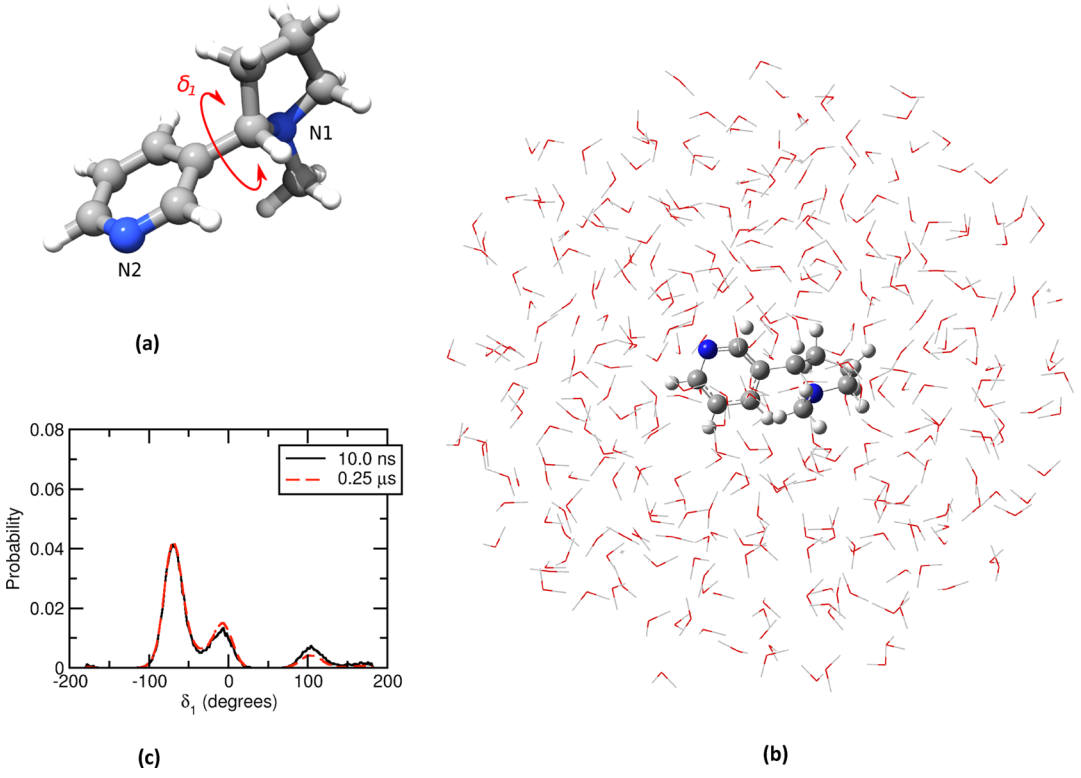

Figure 16. (a) Nicotine structure and definition of the δ_1 dihedral angle, defining the conformers. (b) A random snapshot selected from the MD simulation of nicotine in aqueous solution. (c) Conformational analysis extracted from MD.[95]

which is almost spherical, the majority of the relevant FQ molecules are shared by more than a single QM atom. MLAT has a more extended structure: therefore, increasing the R value causes new independent relevant FQ molecules to be included in the calculation.

Figure 13 also reports E_{rep} values obtained by using the KM-EDA approach. The error between our values and the reference KM-EDA data is about 9% for MOXY, and about 20% for MLAT. These findings confirm the applicability of our procedure to molecular systems in aqueous solution, in fact the calculated errors are of the same magnitude as what has been previously reported for water dimers (see Figure 8). Table S7 in the SI gives a more detailed comparison between our calculated values, KM-EDA data, and what can be obtained by exploiting the EFP2 approach.

6.1. Nicotine in Aqueous Solution. To end the section on the numerical testing of the developed procedure, the approach reported in this paper is applied to nicotine in aqueous solution (Figure 16, panel a)).

Starting from the MD performed previously by some of the present authors,[95] 300 snapshots were selected (more details on the MD protocol and the procedure for the extraction of the snapshots are given in the SI, section S5.1). The QM portion of the system was then described at the CAM-B3LYP/6-31+G* level of theory, according to previous studies on this molecule.[95,127] Figure 16, panel b) depicts a randomly selected snapshot taken from the MD of Nicotine in aqueous solution.

The analysis of the MD trajectory[95] shows that nicotine exhibits 3 different conformers in aqueous solution: the A conformer, having an average value of δ_1 = 106.4 degrees, the B conformer (δ_1 = −65 degrees) and the 0 conformer, where δ_1 = 0 degrees. Figure 16, panel (c) shows the distribution of each conformer obtained from the MD simulation.[127] The most populated conformers belong to the B family, followed by the 0 and A families. Also, the analysis of the MD trajectory[95] shows that at least two water molecules are bound to nicotine nitrogen atoms through hydrogen-bonding interactions.

The distribution in panel (c) of Figure 16 is maintained in the 300 snapshots selected in this study, for which E_{rep}, E_{dis} and consequently E_{Qnel} were calculated. The resulting values of such energies are reported in the Figure 17 as a function of the snapshot. On the basis of the values depicted in Figure 13, E_{rep} was calculated by imposing the R = 5 Å, which in the present case implies on average 52 water molecules to be considered in the evaluation of this term.

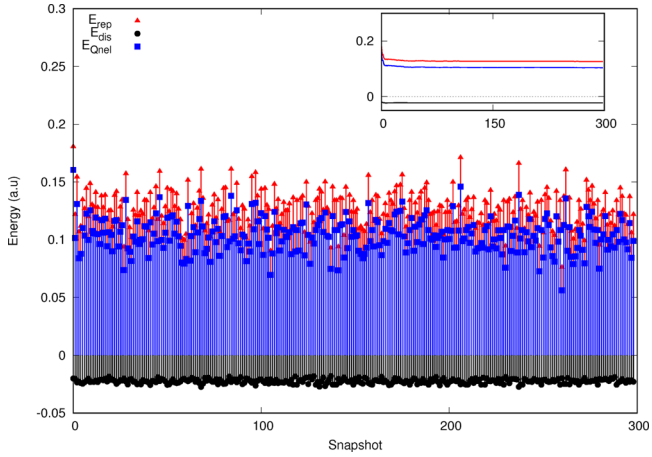

Figure 17. Calculated E_{rep}, E_{dis}, and E_{Qnel} as a function of the snapshot for nicotine in aqueous solution. The trends in average values as a function of the snapshot are given in the inset.

DOI: 10.1021/acs.jctc.7b00776
J. Chem. Theory Comput. 2017, 13, 4854−4870

Figure 17 clearly shows that, as previously reported by some of the present authors for other molecular properties,[13,24,49] E_{rep}, E_{dis} and E_{Qnel} may differ as a function of the snapshot. E_{Qnel} is always positive, showing that the attractive, negative, E_{dis} terms is always smaller than the repulsive, positive E_{rep} contribution. The average value of the three terms as a function of the snapshot is depicted as inset in Figure 17. Clearly, convergence is reached very quickly, when only 80 snapshots are considered, that different from other investigated properties of this and other molecular systems, requiring hundreds or thousands of snapshots to get a fully converged value for molecular spectral properties.[13,24,49]

To refine the analysis, the 300 snapshots were assigned to the three different conformers, that in order to dissect the role of the different E_{rep} and E_{dis} terms in each subclass of structures. To this end, a snapshot was considered to belong to the A family of conformers if $70 < \delta_1 < 180$, B conformers if $-180 < \delta_1 < -40$ and 0 conformers otherwise. This partitioning allows the snapshots to be divided in subclasses of structures and the contributions for each class to be calculated. The results of this analysis are summarized in Table 6, where also standard deviations are reported.

Table 6. Calculated E_{rep}, E_{dis}, and E_{Qnel} for Nicotine in Aqueous Solution[a]

conformer	E_{rep}	E_{dis}	E_{Qnel}	ΔE_{Qnel}
A	12.8 (±1.5)	−2.2 (±0.1)	10.6(±1.5)	0.4 (2.4 kcal/mol)
B	12.6 (±1.7)	−2.2 (±0.2)	10.4(±1.6)	0.2 (1.2 kcal/mol)
0	12.4 (±1.1)	−2.2 (±0.1)	10.2(±1.1)	0.0

[a] ΔE_{Qnel} is the non-electrostatic energy difference between the various conformers and the most stabilized one (0). All data are given in 10^{-2} Hartree unless differently stated and refer to 300 selected snapshots. Standard deviations are reported in parentheses.

Table 6 clearly shows that the calculated E_{Qnel} values are similar for the three conformers, and they do not differ statistically. In particular, the lowest E_{Qnel} is exhibited by conformer 0, due to the fact that this conformer shows the lowest value of E_{rep} in combination with a rather small absolute value of E_{dis}. As it has been noticed by some of us in previous works,[95] the analysis of the MD shows that the 0 conformer is characterized by a short lifetime (10 ps), and this is due to the weak hydrogen bonding pattern exhibited by this conformer with respect to the other two. Therefore, the nearest water molecules are placed farther than in the two other cases, thus giving rise to lower E_{rep} values.

The total nonelectrostatic energy difference of the various conformers with respect to 0 is reported in the last column of Table 6. The values are small, but not negligible, and in particular their magnitude is such to potentially affect the predicted conformational weights in aqueous solutions.

In Table 7, the average dipole moments calculated by exploiting the three QM/TIP3P, QM/FQ and QM/FQ + Quantum nonelectrostatic interactions approaches are reported. The difference between the dipole obtained by including polarization effects is huge, as expected (an increase of about 50% is observed). The third column in Table 7 shows the dipole moment calculated by using the QM/FQ approach coupled with our description of repulsive and dispersive interactions. By referring again to Table 6 and Figure 17, we note again that the repulsion term is dominant if compared to the dispersion. This results in a confinement of the molecular density, which causes the decrease of the molecular dipole, as expected.

Table 7. Calculated Dipole Moment of Nicotine in Aqueous Solution, Obtained by Exploiting Nonpolarizable (QM/TIP3P), Polarizable (QM/FQ), and polarizable + Nonelectrostatic (QM/FQ + Qnel) Approaches[a]

$\mu_{QM/TIP3P}$	$\mu_{QM/FQ}$	$\mu_{QM/FQ+Qnel}$
3.1	5.9	4.2

[a] All data are given in Debye and refer to 300 selected snapshots.

7. SUMMARY, CONCLUSIONS, AND FUTURE PERSPECTIVES

In this paper, a general route to calculate quantum repulsion and quantum dispersion effects in polarizable and nonpolarizable QM/MM approaches has been formulated. A remarkable peculiarity of the proposed approach is that repulsion/dispersion contributions are explicitly introduced in the QM Hamiltonian. Therefore, such terms not only enter the evaluation of the energetic properties of the systems but, remarkably, can be propagated to the calculation of molecular properties and spectra. Due to the specific form of the contributions, a reliable yet extensive application of the methodology requires a compulsory parametrization for different MM substrates, however the number of parameters entering the definition of our method is remarkably low. In this paper, a parametrization for the aqueous solution, which is the natural environment for most biomolecules, is proposed. Such a parametrization is able to reproduce the most important features of the aqueous solution, for which the reported data are in good agreement with reference data. The application of the obtained parametrization to the calculation of the nonelectrostatic interaction energy of aqueous nicotine shows that the Pauli repulsion contribution is larger than the dispersion term for all the representative snapshots extracted from the MD. This feature can potentially impact QM/MM geometry optimization of molecular systems in aqueous solution, which are currently performed by only resorting to the electrostatic term.[48] The results of this study pave the way to similar studies, aimed at extending the parametrization to environments other that water, in which nonelectrostatic terms can compare (or even overcome) with the generally dominating electrostatic component of the molecule-environment interaction. Such studies, and the related parametrizations, together with the extension of our method to the calculation of molecular properties and spectroscopies, will be the topic of future communications.

■ ASSOCIATED CONTENT

Supporting Information

The Supporting Information is available free of charge on the ACS Publications website at DOI: 10.1021/acs.jctc.7b00776.

Obara-Saika algorithm for the evaluation of A_μ in eq 9; results of the parametrization of eq 29; quantum dispersion parameters; raw data for the dependence of E_{rep}, E_{dis}, and E_{Qnel} on the QM description; detailed comparison between our calculated values; KM-EDA and EFP2 approach for MLAT and MOXY in aqueous solution; details on the MD protocol used for nicotine in aqueous solution (PDF)

DOI: 10.1021/acs.jctc.7b00776
J. Chem. Theory Comput. 2017, 13, 4854−4870

AUTHOR INFORMATION

Corresponding Author

*E-mail: chiara.cappelli@sns.it.

ORCID

Tommaso Giovannini: 0000-0002-5637-2853
Chiara Cappelli: 0000-0002-4872-4505

Notes

The authors declare no competing financial interest.

ACKNOWLEDGMENTS

The authors thank Giovanni Scalmani for useful discussion on implementation issues.

REFERENCES

(1) Warshel, A.; Levitt, M. Theoretical studies of enzymic reactions: Dielectric, electrostatic and steric stabilization of the carbonium ion in the reaction of lysozyme. *J. Mol. Biol.* **1976**, *103*, 227−249.

(2) Field, M. J.; Bash, P. A.; Karplus, M. A combined quantum mechanical and molecular mechanical potential for molecular dynamics simulations. *J. Comput. Chem.* **1990**, *11*, 700−733.

(3) Gao, J. Hybrid quantum and molecular mechanical simulations: an alternative avenue to solvent effects in organic chemistry. *Acc. Chem. Res.* **1996**, *29*, 298−305.

(4) Giese, T. J.; York, D. M. Improvement of semiempirical response properties with charge-dependent response density. *J. Chem. Phys.* **2005**, *123*, 164108.

(5) Giese, T. J.; York, D. M. Charge-dependent model for many-body polarization, exchange, and dispersion interactions in hybrid quantum mechanical/ molecular mechanical calculations. *J. Chem. Phys.* **2007**, *127*, 194101.

(6) Friesner, R. A.; Guallar, V. Ab initio quantum chemical and mixed quantum mechanics/molecular mechanics (QM/MM) methods for studying enzymatic catalysis. *Annu. Rev. Phys. Chem.* **2005**, *56*, 389−427.

(7) Lin, H.; Truhlar, D. G. QM/MM: what have we learned, where are we, and where do we go from here? *Theor. Chem. Acc.* **2007**, *117*, 185.

(8) Senn, H. M.; Thiel, W. QM/MM methods for biomolecular systems. *Angew. Chem., Int. Ed.* **2009**, *48*, 1198−1229.

(9) Monari, A.; Rivail, J.-L.; Assfeld, X. Theoretical modeling of large molecular systems. Advances in the local self consistent field method for mixed quantum mechanics/molecular mechanics calculations. *Acc. Chem. Res.* **2013**, *46*, 596−603.

(10) Woo, T.; Margl, P.; Deng, L.; Cavallo, L.; Ziegler, T. Towards more realistic computational modeling of homogenous catalysis by density functional theory: combined QM/MM and ab initio molecular dynamics. *Catal. Today* **1999**, *50*, 479−500.

(11) Warshel, A. Computer simulations of enzyme catalysis: methods, progress, and insights. *Annu. Rev. Biophys. Biomol. Struct.* **2003**, *32*, 425−443.

(12) Sinnecker, S.; Neese, F. QM/MM calculations with DFT for taking into account protein effects on the EPR and optical spectra of metalloproteins. Plastocyanin as a case study. *J. Comput. Chem.* **2006**, *27*, 1463−1475.

(13) Lipparini, F.; Egidi, F.; Cappelli, C.; Barone, V. The optical rotation of methyloxirane in aqueous solution: a never ending story? *J. Chem. Theory Comput.* **2013**, *9*, 1880−1884.

(14) Mennucci, B. Modeling environment effects on spectroscopies through QM/classical models. *Phys. Chem. Chem. Phys.* **2013**, *15*, 6583−6594.

(15) De Mitri, N.; Monti, S.; Prampolini, G.; Barone, V. Absorption and emission spectra of a flexible dye in solution: a computational time-dependent approach. *J. Chem. Theory Comput.* **2013**, *9*, 4507−4516.

(16) Shaik, S.; Cohen, S.; Wang, Y.; Chen, H.; Kumar, D.; Thiel, W. P450 Enzymes: Their Structure, Reactivity, and Selectivity Modeled by QM/MM Calculations. *Chem. Rev.* **2010**, *110*, 949−1017.

(17) Cavalli, A.; Carloni, P.; Recanatini, M. Target-related applications of first principles quantum chemical methods in drug design. *Chem. Rev.* **2006**, *106*, 3497−3519.

(18) Carnimeo, I.; Cappelli, C.; Barone, V. Analytical gradients for MP2, double hybrid functionals, and TD-DFT with polarizable embedding described by fluctuating charges. *J. Comput. Chem.* **2015**, *36*, 2271−2290.

(19) Lodola, A.; De Vivo, M. The increasing role of QM/MM in drug discovery. *Adv. Protein Chem. Struct. Biol.* **2012**, *87*, 337−362.

(20) Gordon, M. S.; Slipchenko, L.; Li, H.; Jensen, J. H. The effective fragment potential: a general method for predicting intermolecular interactions. Annu. *Annu. Rep. Comput. Chem.* **2007**, *3*, 177−193.

(21) Jacquemin, D.; Perpète, E. A.; Laurent, A. D.; Assfeld, X.; Adamo, C. Spectral properties of self-assembled squaraine-tetralactam: a theoretical assessment. *Phys. Chem. Chem. Phys.* **2009**, *11*, 1258−1262.

(22) Monari, A.; Very, T.; Rivail, J.-L.; Assfeld, X. A QM/MM study on the spinach plastocyanin: redox properties and absorption spectra. *Comput. Theor. Chem.* **2012**, *990*, 119−125.

(23) Jurinovich, S.; Curutchet, C.; Mennucci, B. The Fenna-Matthews-Olson Protein Revisited: A Fully Polarizable (TD) DFT/MM Description. *ChemPhysChem* **2014**, *15*, 3194−3204.

(24) Giovannini, T.; Olszowka, M.; Cappelli, C. Effective Fully Polarizable QM/MM Approach To Model Vibrational Circular Dichroism Spectra of Systems in Aqueous Solution. *J. Chem. Theory Comput.* **2016**, *12*, 5483−5492.

(25) Bakowies, D.; Thiel, W. Hybrid models for combined quantum mechanical and molecular mechanical approaches. *J. Phys. Chem.* **1996**, *100*, 10580−10594.

(26) Rick, S. W.; Stuart, S. J.; Berne, B. J. Dynamical fluctuating charge force fields: Application to liquid water. *J. Chem. Phys.* **1994**, *101*, 6141−6156.

(27) Lipparini, F.; Barone, V. Polarizable force fields and polarizable continuum model: a fluctuating charges/PCM approach. 1. theory and implementation. *J. Chem. Theory Comput.* **2011**, *7*, 3711−3724.

(28) Day, P. N.; Jensen, J. H.; Gordon, M. S.; Webb, S. P.; Stevens, W. J.; Krauss, M.; Garmer, D.; Basch, H.; Cohen, D. An effective fragment method for modeling solvent effects in quantum mechanical calculations. *J. Chem. Phys.* **1996**, *105*, 1968−1986.

(29) Kairys, V.; Jensen, J. H. QM/MM boundaries across covalent bonds: a frozen localized molecular orbital-based approach for the effective fragment potential method. *J. Phys. Chem. A* **2000**, *104*, 6656−6665.

(30) Mao, Y.; Demerdash, O.; Head-Gordon, M.; Head-Gordon, T. Assessing Ion-Water Interactions in the AMOEBA Force Field Using Energy Decomposition Analysis of Electronic Structure Calculations. *J. Chem. Theory Comput.* **2016**, *12*, 5422−5437.

(31) Thole, B. T. Molecular polarizabilities calculated with a modified dipole interaction. *Chem. Phys.* **1981**, *59*, 341−350.

(32) Steindal, A. H.; Ruud, K.; Frediani, L.; Aidas, K.; Kongsted, J. Excitation energies in solution: the fully polarizable QM/MM/PCM method. *J. Phys. Chem. B* **2011**, *115*, 3027−3037.

(33) Boulanger, E.; Thiel, W. Solvent boundary potentials for hybrid QM/MM computations using classical drude oscillators: a fully polarizable model. *J. Chem. Theory Comput.* **2012**, *8*, 4527−4538.

(34) Stone, A. *The Theory of Intermolecular Forces*; OUP: Oxford, 2013.

(35) Lennard-Jones, J. E. Cohesion. *Proc. Phys. Soc.* **1931**, *43*, 461.

(36) Sherrill, C. D. *Reviews in Computational Chemistry*; John Wiley & Sons, Inc., 2009; pp 1−38.

(37) Tschumper, G. S. *Reviews in Computational Chemistry*; John Wiley & Sons, Inc., 2009; pp 39−90.

(38) Gordon, M. S.; Freitag, M. A.; Bandyopadhyay, P.; Jensen, J. H.; Kairys, V.; Stevens, W. J. The effective fragment potential method: A QM-based MM approach to modeling environmental effects in chemistry. *J. Phys. Chem. A* **2001**, *105*, 293−307.

(39) Adamovic, I.; Gordon, M. S. Dynamic polarizability, dispersion coefficient C6 and dispersion energy in the effective fragment potential method. *Mol. Phys.* **2005**, *103*, 379−387.

(40) Slipchenko, L. V. *Many-Body Effects and Electrostatics in Biomolecules*; Pan Stanford, 2016; pp 147−187.

DOI: 10.1021/acs.jctc.7b00776
J. Chem. Theory Comput. 2017, 13, 4854−4870

(41) Szalewicz, K. Symmetry-adapted perturbation theory of intermolecular forces. *WIRES: Comput. Mol. Sci.* **2012**, *2*, 254−272.
(42) Hohenstein, E. G.; Sherrill, C. D. Wavefunction methods for noncovalent interactions. *WIRES: Comput. Mol. Sci.* **2012**, *2*, 304−326.
(43) Tkatchenko, A.; Scheffler, M. Accurate molecular van der Waals interactions from ground-state electron density and free-atom reference data. *Phys. Rev. Lett.* **2009**, *102*, 073005.
(44) Tkatchenko, A.; Romaner, L.; Hofmann, O. T.; Zojer, E.; Ambrosch-Draxl, C.; Scheffler, M. Van der Waals interactions between organic adsorbates and at organic/inorganic interfaces. *MRS Bull.* **2010**, *35*, 435−442.
(45) Tkatchenko, A.; DiStasio, R. A., Jr; Car, R.; Scheffler, M. Accurate and efficient method for many-body van der Waals interactions. *Phys. Rev. Lett.* **2012**, *108*, 236402.
(46) Hermann, J.; DiStasio, R. A.; Tkatchenko, A. First-Principles Models for van der Waals Interactions in Molecules and Materials: Concepts, Theory, and Applications. *Chem. Rev.* **2017**, *117*, 4714−4758.
(47) Lipparini, F.; Cappelli, C.; Barone, V. Linear response theory and electronic transition energies for a fully polarizable QM/classical hamiltonian. *J. Chem. Theory Comput.* **2012**, *8*, 4153−4165.
(48) Lipparini, F.; Cappelli, C.; Scalmani, G.; De Mitri, N.; Barone, V. Analytical first and second derivatives for a fully polarizable QM/classical hamiltonian. *J. Chem. Theory Comput.* **2012**, *8*, 4270−4278.
(49) Cappelli, C. Integrated QM/Polarizable MM/Continuum Approaches to Model Chiroptical Properties of Strongly Interacting Solute-Solvent Systems. *Int. J. Quantum Chem.* **2016**, *116*, 1532−1542.
(50) Amovilli, C.; McWeeny, R. A matrix partitioning approach to the calculation of intermolecular potentials. General theory and some examples. *Chem. Phys.* **1990**, *140*, 343−361.
(51) McWeeny, R. *Methods of Molecular Quantum Mechanics*; Academic Press, 1992.
(52) Amovilli, C.; Mennucci, B. Self-consistent-field calculation of Pauli repulsion and dispersion contributions to the solvation free energy in the polarizable continuum model. *J. Phys. Chem. B* **1997**, *101*, 1051−1057.
(53) Tomasi, J.; Mennucci, B.; Cammi, R. Quantum mechanical continuum solvation models. *Chem. Rev.* **2005**, *105*, 2999−3094.
(54) Mennucci, B.; Amovilli, C.; Tomasi, J. On the effect of Pauli repulsion and dispersion on static molecular polarizabilities and hyperpolarizabilities in solution. *Chem. Phys. Lett.* **1998**, *286*, 221−225.
(55) Cammi, R.; Verdolino, V.; Mennucci, B.; Tomasi, J. Towards the elaboration of a QM method to describe molecular solutes under the effect of a very high pressure. *Chem. Phys.* **2008**, *344*, 135−141.
(56) Cammi, R.; Cappelli, C.; Mennucci, B.; Tomasi, J. Calculation and analysis of the harmonic vibrational frequencies in molecules at extreme pressure: Methodology and diborane as a test case. *J. Chem. Phys.* **2012**, *137*, 154112.
(57) Burke, K.; Perdew, J. P.; Ernzerhof, M. Why semilocal functionals work: Accuracy of the on-top pair density and importance of system averaging. *J. Chem. Phys.* **1998**, *109*, 3760−3771.
(58) Iikura, H.; Tsuneda, T.; Yanai, T.; Hirao, K. A long-range correction scheme for generalized-gradient-approximation exchange functionals. *J. Chem. Phys.* **2001**, *115*, 3540−3544.
(59) Henderson, T. M.; Janesko, B. G.; Scuseria, G. E. Generalized gradient approximation model exchange holes for range-separated hybrids. *J. Chem. Phys.* **2008**, *128*, 194105.
(60) Janesko, B. G.; Scuseria, G. E. Local hybrid functionals based on density matrix products. *J. Chem. Phys.* **2007**, *127*, 164117.
(61) Janesko, B. G. Rung 3.5 density functionals: Another step on Jacob's ladder. *Int. J. Quantum Chem.* **2013**, *113*, 83−88.
(62) Janesko, B. G. Comparing modern density functionals for conjugated polymer band structures: Screened hybrid, Minnesota, and Rung 3.5 approximations. *J. Chem. Phys.* **2011**, *134*, 184105.
(63) Janesko, B. G. Rung 3.5 density functionals. *J. Chem. Phys.* **2010**, *133*, 104103.
(64) Janesko, B. G.; Scalmani, G.; Frisch, M. J. Practical auxiliary basis implementation of Rung 3.5 functionals. *J. Chem. Phys.* **2014**, *141*, 034103.
(65) Obara, S.; Saika, A. Efficient recursive computation of molecular integrals over Cartesian Gaussian functions. *J. Chem. Phys.* **1986**, *84*, 3963−3974.
(66) Helgaker, T.; Jorgensen, P.; Olsen, J. *Molecular Electronic-Structure Theory*; John Wiley & Sons, 2014.
(67) Ahlrichs, R. A simple algebraic derivation of the Obara-Saika scheme for general two-electron interaction potentials. *Phys. Chem. Chem. Phys.* **2006**, *8*, 3072−3077.
(68) Operstein, V. Full Müntz Theorem inLp [0, 1]. *J. Approx. Theory* **1996**, *85*, 233−235.
(69) Amovilli, C.; McWeeny, R. Perturbation calculations of molecular interaction energies: an example, HF···HF. *Chem. Phys. Lett.* **1986**, *128*, 11−17.
(70) Grimme, S. Density functional theory with London dispersion corrections. *WIRES: Comput. Mol. Sci.* **2011**, *1*, 211−228.
(71) Klimeš, J.; Michaelides, A. Perspective: Advances and challenges in treating van der Waals dispersion forces in density functional theory. *J. Chem. Phys.* **2012**, *137*, 120901.
(72) Johnson, E. R.; Mackie, I. D.; DiLabio, G. A. Dispersion interactions in density-functional theory. *J. Phys. Org. Chem.* **2009**, *22*, 1127−1135.
(73) Schwabe, T.; Grimme, S. Towards chemical accuracy for the thermodynamics of large molecules: new hybrid density functionals including non-local correlation effects. *Phys. Chem. Chem. Phys.* **2006**, *8*, 4398−4401.
(74) Andersson, Y.; Hult, E.; Rydberg, H.; Apell, P.; Lundqvist, B. I.; Langreth, D. C. *Electronic Density Functional Theory*; Springer, 1998; pp 243−260.
(75) Dion, M.; Rydberg, H.; Schröder, E.; Langreth, D. C.; Lundqvist, B. I. Van der Waals density functional for general geometries. *Phys. Rev. Lett.* **2004**, *92*, 246401.
(76) Thonhauser, T.; Cooper, V. R.; Li, S.; Puzder, A.; Hyldgaard, P.; Langreth, D. C. Van der Waals density functional: Self-consistent potential and the nature of the van der Waals bond. *Phys. Rev. B: Condens. Matter Mater. Phys.* **2007**, *76*, 125112.
(77) Román-Pérez, G.; Soler, J. M. Efficient implementation of a van der Waals density functional: application to double-wall carbon nanotubes. *Phys. Rev. Lett.* **2009**, *103*, 096102.
(78) Vydrov, O. A.; Van Voorhis, T. Nonlocal van der Waals density functional made simple. *Phys. Rev. Lett.* **2009**, *103*, 063004.
(79) Vydrov, O. A.; Van Voorhis, T. Dispersion interactions from a local polarizability model. *Phys. Rev. A: At., Mol., Opt. Phys.* **2010**, *81*, 062708.
(80) Grimme, S. Semiempirical GGA-type density functional constructed with a long-range dispersion correction. *J. Comput. Chem.* **2006**, *27*, 1787−1799.
(81) Grimme, S.; Antony, J.; Ehrlich, S.; Krieg, H. A consistent and accurate ab initio parametrization of density functional dispersion correction (DFT-D) for the 94 elements H-Pu. *J. Chem. Phys.* **2010**, *132*, 154104.
(82) Bader, R. F. W. *Atoms in Molecules A Quantum Theory*; OUP: Oxford, 1990.
(83) Hirshfeld, F. L. Bonded-atom fragments for describing molecular charge densities. *Theor. Chem. Acc.* **1977**, *44*, 129−138.
(84) Johnson, E. R.; Becke, A. D. A post-Hartree−Fock model of intermolecular interactions. *J. Chem. Phys.* **2005**, *123*, 024101.
(85) Olasz, A.; Vanommeslaeghe, K.; Krishtal, A.; Veszprémi, T.; Van Alsenoy, C.; Geerlings, P. The use of atomic intrinsic polarizabilities in the evaluation of the dispersion energy. *J. Chem. Phys.* **2007**, *127*, 224105.
(86) Caprasecca, S.; Jurinovich, S.; Viani, L.; Curutchet, C.; Mennucci, B. Geometry optimization in polarizable QM/MM models: the induced dipole formulation. *J. Chem. Theory Comput.* **2014**, *10*, 1588−1598.
(87) Rick, S. W.; Stuart, S. J.; Bader, J. S.; Berne, B. J. Fluctuating charge force fields for aqueous solutions. *J. Mol. Liq.* **1995**, *65*−*66*, 31−40.
(88) Rick, S. W.; Berne, B. J. Dynamical Fluctuating Charge Force Fields: The Aqueous Solvation of Amides. *J. Am. Chem. Soc.* **1996**, *118*, 672−679.

DOI: 10.1021/acs.jctc.7b00776
J. Chem. Theory Comput. 2017, 13, 4854−4870

(89) Frisch, M. J.; Trucks, G. W.; Schlegel, H. B.; Scuseria, G. E.; Robb, M. A.; Cheeseman, J. R.; Scalmani, G.; Barone, V.; Petersson, G. A.; Nakatsuji, H.; Li, X.; Caricato, M.; Marenich, A. V.; Bloino, J.; Janesko, B. G.; Gomperts, R.; Mennucci, B.; Hratchian, H. P.; Ortiz, J. V.; Izmaylov, A. F.; Sonnenberg, J. L.; Williams-Young, D.; Ding, F.; Lipparini, F.; Egidi, F.; Goings, J.; Peng, B.; Petrone, A.; Henderson, T.; Ranasinghe, D.; Zakrzewski, V. G.; Gao, J.; Rega, N.; Zheng, G.; Liang, W.; Hada, M.; Ehara, M.; Toyota, K.; Fukuda, R.; Hasegawa, J.; Ishida, M.; Nakajima, T.; Honda, Y.; Kitao, O.; Nakai, H.; Vreven, T.; Throssell, K.; Montgomery, J. A., Jr.; Peralta, J. E.; Ogliaro, F.; Bearpark, M. J.; Heyd, J. J.; Brothers, E. N.; Kudin, K. N.; Staroverov, V. N.; Keith, T. A.; Kobayashi, R.; Normand, J.; Raghavachari, K.; Rendell, A. P.; Burant, J. C.; Iyengar, S. S.; Tomasi, J.; Cossi, M.; Millam, J. M.; Klene, M.; Adamo, C.; Cammi, R.; Ochterski, J. W.; Martin, R. L.; Morokuma, K.; Farkas, O.; Foresman, J. B.; Fox, D. J. *Gaussian 16*, revision A.03; Gaussian Inc.: Wallingford, CT, 2016.

(90) Mark, P.; Nilsson, L. Structure and dynamics of the TIP3P, SPC, and SPC/E water models at 298 K. *J. Phys. Chem. A* **2001**, *105*, 9954−9960.

(91) Berendsen, H.; van der Spoel, D.; van Drunen, R. GROMACS: A message-passing parallel molecular dynamics implementation. *Comput. Phys. Commun.* **1995**, *91*, 43−56.

(92) Lindahl, E.; Hess, B.; van der Spoel, D. GROMACS 3.0: a package for molecular simulation and trajectory analysis. *J. Mol. Model.* **2001**, *7*, 306−317.

(93) Van Der Spoel, D.; Lindahl, E.; Hess, B.; Groenhof, G.; Mark, A. E.; Berendsen, H. J. C. GROMACS: Fast, flexible, and free. *J. Comput. Chem.* **2005**, *26*, 1701−1718.

(94) Hess, B.; Kutzner, C.; van der Spoel, D.; Lindahl, E. GROMACS 4: Algorithms for Highly Efficient, Load-Balanced, and Scalable Molecular Simulation. *J. Chem. Theory Comput.* **2008**, *4*, 435−447.

(95) Egidi, F.; Russo, R.; Carnimeo, I.; D'Urso, A.; Mancini, G.; Cappelli, C. The Electronic Circular Dichroism of Nicotine in Aqueous Solution: A Test Case for Continuum and Mixed Explicit-Continuum Solvation Approaches. *J. Phys. Chem. A* **2015**, *119*, 5396−5404.

(96) Kitaura, K.; Morokuma, K. A new energy decomposition scheme for molecular interactions within the Hartree-Fock approximation. *Int. J. Quantum Chem.* **1976**, *10*, 325−340.

(97) Morokuma, K.; Kitaura, K. *Chemical Applications of Atomic and Molecular Electrostatic Potentials*; Springer, 1981; pp 215−242.

(98) Schmidt, M. W.; Baldridge, K. K.; Boatz, J. A.; Elbert, S. T.; Gordon, M. S.; Jensen, J. H.; Koseki, S.; Matsunaga, N.; Nguyen, K. A.; Su, S.; Windus, T. L.; Dupuis, M.; Montgomery, J. A. General atomic and molecular electronic structure system. *J. Comput. Chem.* **1993**, *14*, 1347−1363.

(99) Gordon, M. S.; Schmidt, M. W. *Theory and Applications of Computational Chemistry: The First Forty Years*; Elsevier, 2005; pp 1167−1189.

(100) Parrish, R. M.; Burns, L. A.; Smith, D. G. A.; Simmonett, A. C.; DePrince, A. E.; Hohenstein, E. G.; Bozkaya, U.; Sokolov, A. Y.; Di Remigio, R.; Richard, R. M.; Gonthier, J. F.; James, A. M.; McAlexander, H. R.; Kumar, A.; Saitow, M.; Wang, X.; Pritchard, B. P.; Verma, P.; Schaefer, H. F.; Patkowski, K.; King, R. A.; Valeev, E. F.; Evangelista, F. A.; Turney, J. M.; Crawford, T. D.; Sherrill, C. D. Psi4 1.1: An Open-Source Electronic Structure Program Emphasizing Automation, Advanced Libraries, and Interoperability. *J. Chem. Theory Comput.* **2017**, *13*, 3185−3197.

(101) Giovannini, T.; Olszówka, M.; Egidi, F.; Cheeseman, J. R.; Scalmani, G.; Cappelli, C. Polarizable Embedding Approach for the Analytical Calculation of Raman and Raman Optical Activity Spectra of Solvated Systems. *J. Chem. Theory Comput.* **2017**, *13*, 4421.

(102) Abascal, J. L.; Vega, C. A general purpose model for the condensed phases of water: TIP4P/2005. *J. Chem. Phys.* **2005**, *123*, 234505.

(103) Boys, S. F. Construction of some molecular orbitals to be approximately invariant for changes from one molecule to another. *Rev. Mod. Phys.* **1960**, *32*, 296.

(104) Jensen, J. H.; Gordon, M. S. An approximate formula for the intermolecular Pauli repulsion between closed shell molecules. *Mol. Phys.* **1996**, *89*, 1313−1325.

(105) Jensen, J. H.; Gordon, M. S. An approximate formula for the intermolecular Pauli repulsion between closed shell molecules. II. Application to the effective fragment potential method. *J. Chem. Phys.* **1998**, *108*, 4772−4782.

(106) Thierfelder, C.; Assadollahzadeh, B.; Schwerdtfeger, P.; Schäfer, S.; Schäfer, R. Relativistic and electron correlation effects in static dipole polarizabilities for the group-14 elements from carbon to element Z= 114: Theory and experiment. *Phys. Rev. A: At., Mol., Opt. Phys.* **2008**, *78*, 052506.

(107) Chu, X.; Dalgarno, A. Linear response time-dependent density functional theory for van der Waals coefficients. *J. Chem. Phys.* **2004**, *121*, 4083−4088.

(108) Chu, X.; Dalgarno, A.; Groenenboom, G. C. Dynamic polarizabilities of rare-earth-metal atoms and dispersion coefficients for their interaction with helium atoms. *Phys. Rev. A: At., Mol., Opt. Phys.* **2007**, *75*, 032723.

(109) Bondi, A. van der Waals volumes and radii. *J. Phys. Chem.* **1964**, *68*, 441−451.

(110) Eisenberg, D.; Kauzmann, W. *The Structure and Properties of Water*; Oxford University Press on Demand, 2005.

(111) Guidez, E. B.; Gordon, M. S. Dispersion Interactions in Water Clusters. *J. Phys. Chem. A* **2017**, *121*, 3736.

(112) Su, P.; Li, H. Energy decomposition analysis of covalent bonds and intermolecular interactions. *J. Chem. Phys.* **2009**, *131*, 014102.

(113) Mancini, G.; Brancato, G.; Barone, V. Combining the Fluctuating Charge Method, Non-Periodic Boundary Conditions and Meta-Dynamics: Aqua Ions as Case Studies. *J. Chem. Theory Comput.* **2014**, *10*, 1150−1163.

(114) Kratz, E. G.; Walker, A. R.; Lagardère, L.; Lipparini, F.; Piquemal, J.-P.; Andrés Cisneros, G. LICHEM: A QM/MM program for simulations with multipolar and polarizable force fields. *J. Comput. Chem.* **2016**, *37*, 1019−1029.

(115) Temelso, B.; Archer, K. A.; Shields, G. C. Benchmark structures and binding energies of small water clusters with anharmonicity corrections. *J. Phys. Chem. A* **2011**, *115*, 12034−12046.

(116) Egidi, F.; Carnimeo, I.; Cappelli, C. Optical rotatory dispersion of methyloxirane in aqueous solution: assessing the performance of density functional theory in combination with a fully polarizable QM/MM/PCMapproach. *Opt. Mater. Express* **2015**, *5*, 196−209.

(117) Jacquemin, D.; Moore, B.; Planchat, A.; Adamo, C.; Autschbach, J. Performance of an optimally tuned range-separated hybrid functional for 0−0 electronic excitation energies. *J. Chem. Theory Comput.* **2014**, *10*, 1677−1685.

(118) Becke, A. D. Density-functional thermochemistry. V. Systematic optimization of exchange-correlation functionals. *J. Chem. Phys.* **1997**, *107*, 8554−8560.

(119) Schmider, H. L.; Becke, A. D. Optimized density functionals from the extended G2 test set. *J. Chem. Phys.* **1998**, *108*, 9624−9631.

(120) Becke, A. D. Density-functional thermochemistry. III. The role of exact exchange. *J. Chem. Phys.* **1993**, *98*, 5648−5652.

(121) Perdew, J. P.; Chevary, J. A.; Vosko, S. H.; Jackson, K. A.; Pederson, M. R.; Singh, D. J.; Fiolhais, C. Atoms, molecules, solids, and surfaces: Applications of the generalized gradient approximation for exchange and correlation. *Phys. Rev. B: Condens. Matter Mater. Phys.* **1992**, *46*, 6671.

(122) Zhao, Y.; Truhlar, D. G. The M06 suite of density functionals for main group thermochemistry, thermochemical kinetics, noncovalent interactions, excited states, and transition elements: two new functionals and systematic testing of four M06-class functionals and 12 other functionals. *Theor. Chem. Acc.* **2008**, *120*, 215−241.

(123) Adamo, C.; Barone, V. Toward reliable density functional methods without adjustable parameters: The PBE0 model. *J. Chem. Phys.* **1999**, *110*, 6158−6170.

(124) Peverati, R.; Truhlar, D. G. Communication: A global hybrid generalized gradient approximation to the exchange-correlation func-

DOI: 10.1021/acs.jctc.7b00776
J. Chem. Theory Comput. 2017, 13, 4854−4870

tional that satisfies the second-order density-gradient constraint and has broad applicability in chemistry. *J. Chem. Phys.* **2011**, *135*, 191102.
(125) Yanai, T.; Tew, D. P.; Handy, N. C. A new hybrid exchange-correlation functional using the Coulomb-attenuating method (CAM-B3LYP). *Chem. Phys. Lett.* **2004**, *393*, 51−57.
(126) Chai, J.-D.; Head-Gordon, M. Long-range corrected hybrid density functionals with damped atom-atom dispersion corrections. *Phys. Chem. Chem. Phys.* **2008**, *10*, 6615−6620.
(127) Egidi, F.; Segado, M.; Koch, H.; Cappelli, C.; Barone, V. A benchmark study of electronic excitation energies, transition moments, and excited-state energy gradients on the nicotine molecule. *J. Chem. Phys.* **2014**, *141*, 224114.

DOI: 10.1021/acs.jctc.7b00776
J. Chem. Theory Comput. 2017, 13, 4854−4870